

Partial wave analysis of $\psi(3686) \rightarrow \Lambda\bar{\Sigma}^0\pi^0 + c.c.$



The BESIII collaboration

E-mail: besiii-publications@ihep.ac.cn

ABSTRACT: Based on a sample of $(2712.4 \pm 14.3) \times 10^6$ $\psi(3686)$ events collected with the BESIII detector, a partial wave analysis of the decay $\psi(3686) \rightarrow \Lambda\bar{\Sigma}^0\pi^0 + c.c.$ is performed to investigate Λ^* and Σ^* resonances in the $\pi^0\bar{\Sigma}^0$ and $\pi^0\Lambda$ invariant mass distributions. Significant contributions are found from the $\Lambda(1405)$, $\Lambda(1520)$, $\Lambda(1600)$, $\Lambda(1670)$, $\Lambda(1690)$, $\Lambda(1800)$, $\Lambda(1890)$, $\Lambda(2325)$, $\Sigma(1385)$, $\Sigma(1660)$, $\Sigma(1670)$, $\Sigma(1750)$, and $\Sigma(1910)$. The masses, widths, and production branching fractions for each component are determined. In addition, the branching fraction of $\psi(3686) \rightarrow \Lambda\bar{\Sigma}^0\pi^0 + c.c.$ is measured to be $(1.544 \pm 0.013 \pm 0.069) \times 10^{-4}$ for the first time, where the first uncertainty is statistical and the second systematic.

Contents

1	Introduction	1
2	BESIII detector and Monte Carlo simulation	2
3	Event Selection	2
4	Background study	4
5	Branching fraction	4
6	Partial wave analysis	6
6.1	Helicity formalism	6
6.2	Nominal fit results	8
6.3	Branching fractions	12
7	Systematic uncertainties	12
7.1	Systematic uncertainties on branching fraction	12
7.2	Systematic uncertainties on partial wave analysis	14
8	Summary	16

1 Introduction

The baryons, composed of three quarks, offer the simplest system in which the three colors of quantum-chromodynamics (QCD) neutralize into colorless objects. Therefore, baryon spectroscopy can be used to shed light on QCD. Although the quark model and lattice QCD have achieved significant success in the interpretation of many properties of baryons and their excited states [1], our current knowledge of baryon spectroscopy is still limited as many fundamental issues are not well understood [2]. In recent years, there have been many studies of excited states of the nucleons, but there are few results on baryons with a strange quark, namely the Λ and Σ hyperons.

In studies of the excited baryons, major difficulties arise from their broad widths and nearby masses, causing a significant amount of overlap between the various excited states. The partial wave analysis (PWA) technique helps to overcome these difficulties by disentangling different resonances using their spin-parity. In the process, their masses, widths, and partial decay widths can be measured.

The large data samples of J/ψ and $\psi(3686)$ events produced from e^+e^- annihilation at BESIII provide excellent opportunities to study different excited baryons. In particular, the $\psi(3686)$, which benefits from having a higher mass than the J/ψ , has more phase

space available in its decays and thus higher mass resonances can be observed. At present, $(2712.4 \pm 14.3) \times 10^6$ $\psi(3686)$ events [3] are now available, which allows us to perform extensive studies of baryon spectroscopy. In this paper, a PWA of the decay $\psi(3686) \rightarrow \Lambda\bar{\Sigma}^0\pi^0 + c.c.$ is performed to investigate potential excited states of the Λ and Σ hyperons. Throughout this paper, the charge-conjugate process is always implied.

2 BESIII detector and Monte Carlo simulation

The BESIII detector [4] records symmetric e^+e^- collisions provided by the BEPCII storage ring [5] in the center-of-mass energy range from 2.0 to 4.95 GeV, with a peak luminosity of $1.1 \times 10^{33} \text{ cm}^{-2}\text{s}^{-1}$ achieved at $\sqrt{s} = 3.773$ GeV. BESIII has collected large data samples in this energy region [6, 7]. The cylindrical core of the BESIII detector covers 93% of the full solid angle and consists of a helium-based multilayer drift chamber (MDC), a plastic scintillator time-of-flight system (TOF), and a CsI(Tl) electromagnetic calorimeter (EMC), which are all enclosed in a superconducting solenoidal magnet providing a 1.0 T magnetic field. The solenoid is supported by an octagonal flux-return yoke with resistive plate counter muon identification modules interleaved with steel. The charged-particle momentum resolution at 1 GeV/c is 0.5%, and the dE/dx resolution is 6% for electrons from Bhabha scattering. The EMC measures photon energies with a resolution of 2.5% (5%) at 1 GeV in the barrel (end cap) region. The time resolution in the TOF barrel region is 68 ps, while that in the end cap region was 110 ps. The end cap TOF system was upgraded in 2015 using multigap resistive plate chamber technology, providing a time resolution of 60 ps, which benefits 83.3% of the data used in this analysis [8–10].

Simulated data samples produced with a GEANT4-based [11] Monte Carlo (MC) package, which includes the geometric description of the BESIII detector and the detector response, are used to determine detection efficiencies and to estimate backgrounds. The simulation models the beam energy spread and initial state radiation (ISR) in the e^+e^- annihilations with the generator KKMC [12, 13]. The inclusive MC sample includes the production of the $\psi(3686)$ resonance, the ISR production of the J/ψ , and the continuum processes incorporated in KKMC [12, 13]. All particle decays are modelled with EVTGEN [14, 15] using branching fractions either taken from the Particle Data Group (PDG) [16], when available, or otherwise estimated with LUNDCHARM [17, 18]. Final state radiation from charged final state particles is incorporated using the PHOTOS package [19].

3 Event Selection

The decay $\psi(3686) \rightarrow \Lambda\bar{\Sigma}^0\pi^0$ is reconstructed using the decays $\Sigma^0 \rightarrow \Lambda\gamma$, $\Lambda \rightarrow p\pi^-$, and $\pi^0 \rightarrow \gamma\gamma$. Since the final state of the signal decay is $p\bar{p}\pi^+\pi^-\gamma\gamma\gamma$, the number of charged tracks is required to be four with zero net charge. Each charged track must satisfy $|\cos\theta| < 0.93$, where θ is the polar angle of the track measured by the MDC with respect to the direction of the positron beam. Each of the photon candidates is required to have an energy deposited in the EMC of more than 25 MeV in the barrel ($|\cos\theta| < 0.80$) or 50 MeV in the end-caps ($0.86 < |\cos\theta| < 0.92$). To eliminate showers from charged tracks, the

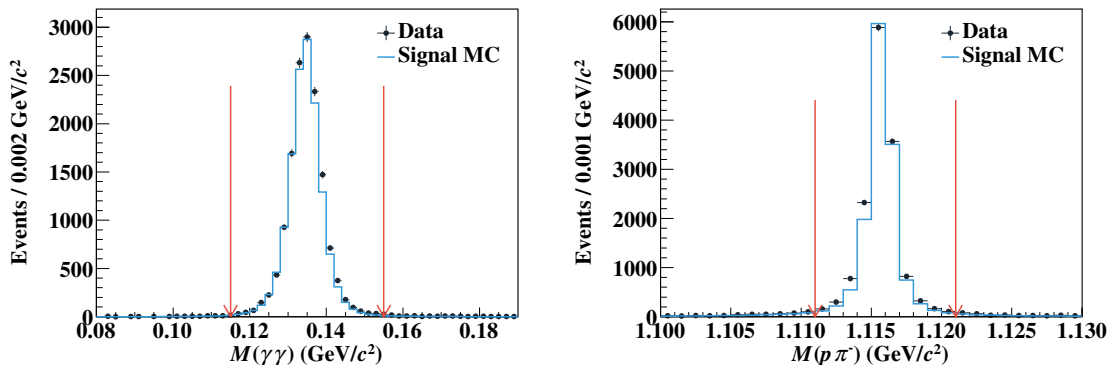


Figure 1: The distributions of $M(\gamma\gamma)$ and $M(p\pi^-)$. The dots with error bars represent data and the blue histograms are the normalized signal MC sample. The signal regions of π^0 and Λ are shown with the red arrows.

opening angle between the position of each shower in the EMC and any charged track must be greater than 10 degrees. To suppress electronic noise and showers unrelated to the event, the EMC time difference from the event start time is required to be within $[0, 700]$ ns. At least three photon candidates are required.

The Λ and $\bar{\Lambda}$ candidates are reconstructed by combining pairs of oppositely charged tracks with pion and proton mass hypotheses, fulfilling a secondary vertex constraint [20]. Events with at least one $\Lambda(p\pi^-)$ candidate and one $\bar{\Lambda}(\bar{p}\pi^+)$ candidate are selected. In the case of multiple $\Lambda\bar{\Lambda}$ pair candidates, the one with the minimum value of $\chi_{\text{s vtx}}^2(\Lambda) + \chi_{\text{s vtx}}^2(\bar{\Lambda})$ is chosen, where $\chi_{\text{s vtx}}^2(\Lambda)$ and $\chi_{\text{s vtx}}^2(\bar{\Lambda})$ are the fit χ^2 of the secondary vertex fits for the Λ and $\bar{\Lambda}$, respectively. To improve the momentum and energy resolution and reduce background, a four-constraint (energy-momentum conservation, 4C) kinematic fit is applied under the hypothesis of $\psi(3686) \rightarrow \Lambda\bar{\Lambda}\gamma\gamma$, and the corresponding fit χ^2 (χ_{4C}^2) is required to be less than 40. For events with more than three photon candidates, the combination with the least χ_{4C}^2 is selected from all possible combinations. To reject possible background events from $\psi(3686) \rightarrow \Lambda\bar{\Lambda}\gamma\gamma$ and $\psi(3686) \rightarrow \Lambda\bar{\Lambda}\gamma\gamma\gamma$, we further require that the χ_{4C}^2 for the $\psi(3686) \rightarrow \Lambda\bar{\Lambda}\gamma\gamma\gamma$ hypothesis is less than those of both the $\psi(3686) \rightarrow \Lambda\bar{\Lambda}\gamma\gamma$ and $\psi(3686) \rightarrow \Lambda\bar{\Lambda}\gamma\gamma\gamma$ hypotheses. In the case of multiple π^0 candidates, the one with the minimum of $\Delta M(\pi^0)$ is chosen. The $\Delta M(\pi^0)$ is defined as $\Delta M(\pi^0) = |M(\gamma_a\gamma_b) - M_{\text{PDG}}(\pi^0)|$, where $M(\gamma_a\gamma_b)$ is the invariant mass of two photon candidates from the 4C kinematic fit and $M_{\text{PDG}}(\pi^0)$ is the nominal π^0 mass [16]. The final distributions of $M(\gamma\gamma)$ and $M(p\pi^-)$ are shown in figure 1, where clear π^0 and Λ signals are observed. The invariant mass of the chosen π^0 candidate is required to be in the π^0 signal region, $0.115 < M(\pi^0) < 0.155$ GeV/c^2 ; and the invariant mass of $p\pi^-$ is required to be in the Λ signal region, $1.111 < M(p\pi^-) < 1.121$ GeV/c^2 .

To suppress mis-combination from the conjugated channel, the invariant mass of $\gamma\Lambda$ from $\psi(3686) \rightarrow \Lambda\bar{\Sigma}^0\pi^0$ is required to not be in the Σ^0 signal region $M(\gamma\Lambda) < 1.179$ GeV/c^2 or $M(\gamma\Lambda) > 1.204$ GeV/c^2 . To reject the peaking background in the Σ^0 signal region

from $\psi(3686) \rightarrow \gamma\chi_{cJ}$, $\chi_{cJ} \rightarrow \Sigma^0\bar{\Sigma}^0$, the requirement $\Delta M(\pi^0\Sigma^0/\pi^0\bar{\Sigma}^0) < \Delta M(\Sigma^0\bar{\Sigma}^0)$ is imposed. Here, $\Delta M(\pi^0\Sigma^0/\pi^0\bar{\Sigma}^0)$ is defined as $\Delta M(\pi^0\Sigma^0/\pi^0\bar{\Sigma}^0) = |(M(\pi^0) - M_{\text{PDG}}(\pi^0))| + |(M(\Sigma^0/\bar{\Sigma}^0) - M_{\text{PDG}}(\Sigma^0))|$, where $M(\pi^0)$ and $M(\Sigma^0/\bar{\Sigma}^0)$ are the invariant masses of the reconstructed π^0 and $\Sigma^0/\bar{\Sigma}^0$, respectively. The $M_{\text{PDG}}(\Sigma^0)$ is the Σ^0 nominal mass [16]. The $\Delta M(\pi^0\Sigma^0/\pi^0\bar{\Sigma}^0)$ is examined by looping over all three photons to reconstruct the π^0 , and the remaining photon is used to reconstruct the $\Sigma^0/\bar{\Sigma}^0$. The $\Delta M(\Sigma^0\bar{\Sigma}^0)$ is defined as $\Delta M(\Sigma^0\bar{\Sigma}^0) = |(M(\Sigma^0) - M_{\text{PDG}}(\Sigma^0))| + |(M(\bar{\Sigma}^0) - M_{\text{PDG}}(\bar{\Sigma}^0))|$, where $M(\Sigma^0)$ and $M(\bar{\Sigma}^0)$ are the invariant masses of the reconstructed Σ^0 and $\bar{\Sigma}^0$, respectively. The $\Delta M(\Sigma^0\bar{\Sigma}^0)$ is examined by looping over all three photons to reconstruct the Σ^0 and $\bar{\Sigma}^0$ simultaneously. After applying all the selection criteria mentioned above, around 17,000 events in data remain.

4 Background study

To investigate the possible background contributions, the same selection criteria are applied to the inclusive MC sample of 2.7 billion $\psi(3686)$ events. An analysis of the surviving events is performed with the generic tool TOPOANA [21]. It is found that the background peaking around the $\Sigma^0/\bar{\Sigma}^0$ nominal mass mainly comes from $\psi(3686) \rightarrow \gamma\chi_{cJ}$, $\chi_{cJ} \rightarrow \Sigma^0\bar{\Sigma}^0$, while the mis-combination and other background sources form a flat distribution. The fraction of the background events from $\psi(3686) \rightarrow \gamma\chi_{cJ}$, $\chi_{cJ} \rightarrow \Sigma^0\bar{\Sigma}^0$, estimated by using the π^0 sideband events, is determined to be 0.8%.

To estimate the background due to continuum production, the same procedure is performed on the data taken at $\sqrt{s} = 3.773$ GeV with an integrated luminosity of 7.9 fb^{-1} [22–24]. The background yield is extracted by an extended unbinned maximum likelihood fit to the $M(\gamma\Lambda/\gamma\bar{\Lambda})$ distribution, and normalized to the $\psi(3686)$ data taking into account the luminosity and energy-dependent cross section. The normalization factor f_c is calculated as

$$f_c = \frac{N_{\psi(3686)}^{\text{obs}}}{N_{\psi(3770)}^{\text{obs}}} = \frac{\mathcal{L}_{\psi(3686)}}{\mathcal{L}_{\psi(3770)}} \cdot \frac{\sigma_{\psi(3686)}}{\sigma_{\psi(3770)}} \cdot \frac{\epsilon_{\psi(3686)}}{\epsilon_{\psi(3770)}}, \quad (4.1)$$

where N^{obs} , \mathcal{L} , σ , and ϵ are the number of observed events, integrated luminosity of data, cross-section, and detection efficiency at each energy point, respectively. The details of the cross-section values can be found in ref. [25]. The ratio of detection efficiencies, $\epsilon_{\psi(3686)}/\epsilon_{\psi(3770)}$, is determined by MC simulation. The scale factor is calculated to be $f_c = 0.50$. After normalization, the background yield from $e^+e^- \rightarrow \Lambda\bar{\Sigma}^0\pi^0$ in the $\psi(3686)$ data is determined to be 235.2 ± 11.3 .

5 Branching fraction

To determine the signal yield, an extended unbinned maximum likelihood fit is performed on the $M(\gamma\Lambda)$ distribution. In the fit, the Σ^0 is described by the signal MC shape convolved with a Gaussian function. The non-peaking and mis-combination backgrounds are parameterized by a first-order Chebychev polynomial function. The continuum background

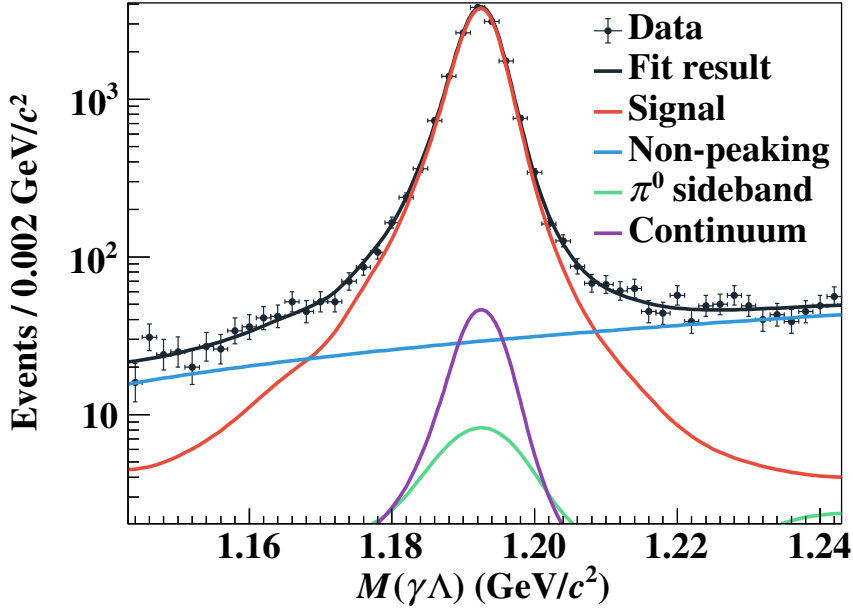


Figure 2: The distribution of $M(\gamma\Lambda)$. The black dots with error bars are data. The black solid curve represents the total fit result, the red solid curve the signal, the blue solid curve the non-peaking background, the green solid curve the π^0 sideband, and the purple solid curve the continuum background.

shape is derived from the data taken at $\sqrt{s} = 3.773$ GeV. The peaking background from $\chi_{cJ} \rightarrow \Sigma^0 \bar{\Sigma}^0$ is estimated by the π^0 sideband defined as $M(\gamma\gamma) \in (0.08, 0.1)$ GeV/ c^2 or $(0.17, 0.19)$ GeV/ c^2 . The number of π^0 sideband events is estimated to be $N_{\pi^0}^{\text{side}} = 126.0 \pm 11.2$, where the uncertainty is statistical only. The fit results are shown in figure 2, from which we obtain 15560.9 ± 131.2 signal events.

With the detection efficiency obtained from the signal MC sample generated with the PWA results, the branching fraction of $\psi(3686) \rightarrow \Lambda \bar{\Sigma}^0 \pi^0$ is determined to be

$$\begin{aligned} \mathcal{B}(\psi(3686) \rightarrow \Lambda \bar{\Sigma}^0 \pi^0 + c.c.) &= \frac{N^{\text{obs}}}{N_{\psi(3686)} \cdot \mathcal{B}^2(\Lambda \rightarrow p\pi^-) \cdot \mathcal{B}(\pi^0 \rightarrow \gamma\gamma) \cdot \mathcal{B}(\Sigma^0 \rightarrow \gamma\Lambda) \cdot \epsilon} \\ &= (1.544 \pm 0.013) \times 10^{-4}, \end{aligned} \quad (5.1)$$

where $N^{\text{obs}} = 15560.9 \pm 131.2$ is the number of signal events in data, $N_{\psi(3686)} = (2712.4 \pm 14.3) \times 10^6$ is the number of $\psi(3686)$ events in data determined with inclusive hadronic events [3], $\epsilon = 9.15\%$ is the detection efficiency obtained from MC simulation, and $\mathcal{B}(\Lambda \rightarrow p\pi^-) = (64.1 \pm 0.5)\%$, $\mathcal{B}(\pi^0 \rightarrow \gamma\gamma) = (98.823 \pm 0.034)\%$, and $\mathcal{B}(\Sigma^0 \rightarrow \gamma\Lambda) = (100)\%$ are the corresponding branching fractions quoted from the PDG [16]. The uncertainty of the branching fraction is statistical only.

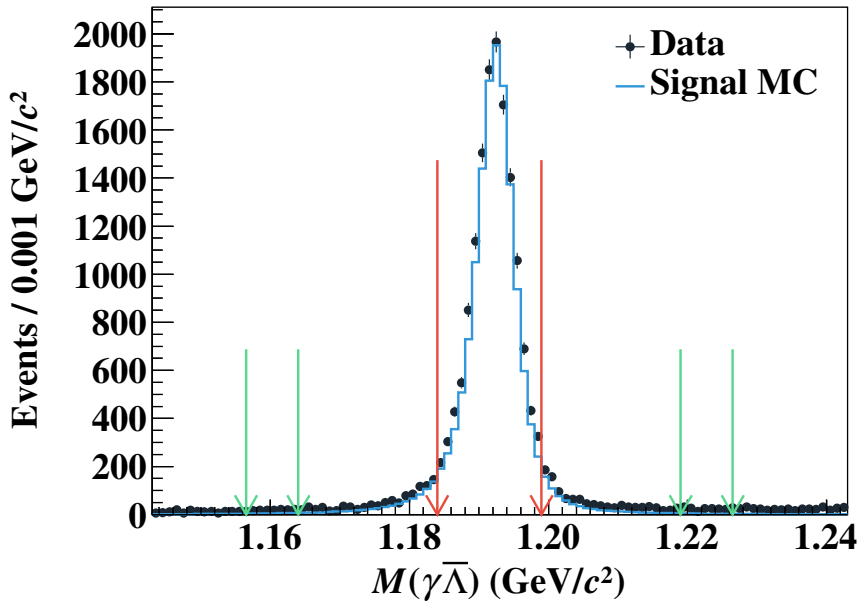


Figure 3: The distribution of $M(\gamma\Lambda)$. The dots with error bars represent data, and the blue histograms are the normalized signal MC sample. The Σ^0 signal regions are shown with the high red arrows and the Σ^0 sideband ranges are shown with the short green arrows.

6 Partial wave analysis

Figure 3 shows the reconstructed mass distribution of the $\gamma\Lambda$ system. To improve the signal purity, an additional requirement on the $\gamma\Lambda$ invariant mass, $1.184 \text{ GeV}/c^2 < M(\gamma\Lambda) < 1.199 \text{ GeV}/c^2$, is applied. After applying all the selection criteria mentioned above, 14,414 events from the $\psi(3686)$ data are selected for the PWA. The Σ^0 sidebands (defined as $M(\gamma\Lambda)$ within $(1.157, 1.164) \text{ GeV}/c^2$ or $(1.219, 1.226) \text{ GeV}/c^2$) and the data at $\sqrt{s} = 3.773 \text{ GeV}$ are used to estimate the yields of the mis-combination and continuum background events, respectively. The numbers of Σ^0 sideband and continuum background events are estimated to be $N_{\Sigma^0}^{\text{side}} = 320.0 \pm 17.9$ and $N^{\text{cont}} = 208.9 \pm 10.1$, respectively. Here, the uncertainties are statistical only. The number of Σ^0 sideband events is fixed with the normalization factor 1.0. Finally, the total number of background events from both sources is 529 after normalization and the signal purity is estimated to be 96.3%. No mass constraint is applied for the final state particles Λ , $\bar{\Sigma}^0$, and π^0 in the PWA. The decay amplitude is constructed using the helicity amplitude formalism, and the full procedure is implemented based on the open-source framework TF-PWA [26].

6.1 Helicity formalism

To construct the full decay amplitude of $\psi(3686) \rightarrow \Lambda \bar{\Sigma}^0 \pi^0$, the helicity formalism is used in conjunction with the isobar model, where the three-body decay is described as a two-step sequential quasi-two-body decay. For each two-body decay $0 \rightarrow 1 + 2$, the helicity amplitude

can be written as

$$A_{\lambda_0, \lambda_1, \lambda_2}^{0 \rightarrow 1+2} = H_{\lambda_1, \lambda_2}^{0 \rightarrow 1+2} D_{\lambda_0, \lambda_1 - \lambda_2}^{J_0^*}(\phi, \theta, 0), \quad (6.1)$$

where the amplitude $H_{\lambda_1, \lambda_2}^{0 \rightarrow 1+2}$ is given by the LS coupling formula [27] along with the barrier factor terms

$$H_{\lambda_1, \lambda_2}^{0 \rightarrow 1+2} = \sum_{l_s} g_{l_s} \sqrt{\frac{2l+1}{2J_0+1}} \langle l0; s\delta | J_0\delta \rangle \langle J_1\lambda_1; J_2 - \lambda_2 | s\delta \rangle q^l B_l'(q, q_0, d), \quad (6.2)$$

where l is the orbital angular momentum, g_{l_s} are the fit parameters, $J_{0,1,2}$ are the spins of particles 0, 1, and 2, $\lambda_{1,2}$ are the helicities for particles 1 and 2, and $\delta = \lambda_1 - \lambda_2$ is the helicity difference. Here, q is the three-momentum modulus of particle 1 in the rest frame of particle 0, which is calculated as

$$q = \frac{\sqrt{[m^2 - (m_1 + m_2)^2][m^2 - (m_1 - m_2)^2]}}{2m}, \quad (6.3)$$

where m , m_1 , and m_2 are the masses of particles 0, 1, and 2, respectively. The normalization factor q_0 is calculated at the nominal resonance mass. The factor $B_l'(q, q_0, d)$ is the reduced Blatt-Weisskopf barrier factor [28]. In the Wigner D -function, $D_{\lambda_0, \lambda_1 - \lambda_2}^{J_0^*}(\phi, \theta, 0)$, ϕ and θ are the helicity angles. The definitions can be found in ref. [29]. The radius d is chosen as $d = 0.73$ fm following ref. [30].

The amplitude for a complete decay chain is constructed as the product of each two body decay amplitude and the resonant propagator R . For example, in the sequential decay $\psi(3686) \rightarrow \Sigma^{*0}\bar{\Sigma}^0$, $\Sigma^{*0} \rightarrow \Lambda\pi^0$, the amplitude is written as

$$A_{\lambda_{\psi(3686)}, \lambda_{\Lambda}, \lambda_{\bar{\Sigma}^0}, \lambda_{\pi^0}}^{\psi(3686) \rightarrow \Sigma^{*0}\bar{\Sigma}^0, \Sigma^{*0} \rightarrow \Lambda\pi^0} = \sum_{\lambda_{\Sigma^{*0}}} A_{\lambda_{\psi(3686)}, \lambda_{\Sigma^{*0}}, \lambda_{\bar{\Sigma}^0}}^{\psi(3686) \rightarrow \Sigma^{*0}\bar{\Sigma}^0} R(m_{\Sigma^{*0}}) A_{\lambda_{\Sigma^{*0}}, \lambda_{\Lambda}, \lambda_{\pi^0}}^{\Sigma^{*0} \rightarrow \Lambda\pi^0}. \quad (6.4)$$

The propagator R includes different models. For all resonances except $\Lambda(1405)$, the relativistic Breit-Wigner formula with mass dependent width is taken as

$$R(m) = \frac{1}{m_0^2 - m^2 - im_0\Gamma(m)}, \quad \Gamma(m) = \Gamma_0 \left(\frac{q}{q_0}\right)^{2l+1} \frac{m_0}{m} B_l'^2(q, q_0, d), \quad (6.5)$$

where Γ_0 is the width of the resonance, and q and q_0 are the momenta in the m and m_0 center-mass-system. The radius d is also chosen as $d = 0.73$ fm following ref. [30].

We describe the two-pole structure of the $\Lambda(1405)$ using the chiral dynamics model [31], which is parameterized as

$$R(m) = \frac{1}{|I - VG|}, \quad (6.6)$$

$$V_{ij}(m) = -C_{ij} \frac{1}{4f^2} (2m - M_i - M_j) \sqrt{\frac{M_i - E_i}{M_i}} \sqrt{\frac{M_j - E_j}{M_j}}, \quad (6.7)$$

$$G_k(m; \mu) = \frac{1}{(4\pi)^2} \left\{ a_k(\mu) + \ln \frac{M_k^2}{\mu} + \frac{m_k^2 - M_k^2 + m^2}{2m^2} \ln \frac{m_k^2}{M_k^2} \right. \\ \left. + \frac{q_k}{m} [\ln(m^2 - (M_k^2 - m_k^2) + 2q_k m) + \ln(m^2 + (M_k^2 - m_k^2) + 2q_k m) \right. \\ \left. - \ln(-m^2 + (M_k^2 - m_k^2) + 2q_k m) - \ln(-m^2 - (M_k^2 - m_k^2) + 2q_k m) \right\}, \quad (6.8)$$

where I is the unit matrix, $m = \sqrt{s}$ is the mass of the event, the C_{ij} coefficients are given in ref. [32], an averaged meson decay constant $f = 1.123f_\pi$ is used [33], with $f_\pi = 92.4$ MeV being the weak pion decay constant, and M_i and E_i are the physical mass and energy of the baryon. The μ is the scale of dimensional regularization fixed to be 630 MeV [33], the subtraction constant $a_k(\mu)$ is quoted from ref. [33], m_i is the physical mass of the meson, and q_k is the momentum in the rest frame of $\Lambda(1405)$.

The construction of the probability density function, the calculation of the fit fraction (FF), and the corresponding statistical uncertainty for each component follow ref. [34]. To consider the effect of mass resolution, we use the method from the TF-PWA documentation [26].

6.2 Nominal fit results

To determine the nominal fit hypothesis of the PWA, the statistical significance of each potential component is evaluated based on the change of the negative log likelihood (NLL) value when that component is included, taking into account the change of the number of degrees of freedom (N_{dof}). The components considered are excited Λ and Σ states, including the $\Lambda(1405)$, $\Lambda(1520)$, $\Lambda(1600)$, $\Lambda(1670)$, $\Lambda(1690)$, $\Lambda(1800)$, $\Lambda(1810)$, $\Lambda(1890)$, $\Lambda(2325)$, $\Sigma(1385)$, $\Sigma(1660)$, $\Sigma(1670)$, $\Sigma(1750)$, and $\Sigma(1910)$ (considered as established by the PDG [16] with a status of at least three stars and a spin less than $5/2$), as well as the $\rho_3(2250)$, $\rho_5(2350)$, and \mathcal{S} -wave non-resonant component (NR_{1-}) in the $M(\Lambda\bar{\Sigma}^0)$ distribution. In addition, an extra Λ state, the $\Lambda(2325)$, is taken into account to describe the high side of the $M(\pi^0\bar{\Sigma}^0)$ distribution. The results show that the resonances $\Lambda(1405)$, $\Lambda(1520)$, $\Lambda(1600)$, $\Lambda(1670)$, $\Lambda(1690)$, $\Lambda(1800)$, $\Lambda(1890)$, $\Lambda(2325)$, $\Sigma(1385)$, $\Sigma(1660)$, $\Sigma(1670)$, $\Sigma(1750)$, and $\Sigma(1910)$ have statistical significance greater than 5σ , while none of the other tested contributions exceed this threshold.

Based on the MC simulation, the mass resolution for the $M(\pi^0\bar{\Sigma}^0)$ distribution is estimated to be 4.8 MeV. The widths of the $\Lambda(1520)$ and $\Lambda(1670)$ states from the PDG [16] are $15 \sim 17$ MeV and $25 \sim 35$ MeV, respectively, which are close to the mass resolution. Therefore, the mass resolution on the $M(\pi^0\bar{\Sigma}^0)$ distribution is taken into account in the nominal fit hypothesis. In the fit, the masses and widths of all resonances are left as free parameters. The obtained masses, widths and fitted fractions of each component are listed in table 1. The invariant mass distributions of $\Lambda\bar{\Sigma}^0$, $\pi^0\Lambda$, and $\pi^0\bar{\Sigma}^0$ are shown in figure 4. The helicity angular distributions are shown in figure 5. The Dalitz plots of $(M(\pi^0\Lambda))^2$ versus $(M(\pi^0\bar{\Sigma}^0))^2$ of data and the PWA fit result are shown in figure 6.

In chiral SU(3) dynamics, the existence of two poles in the $\Lambda(1405)$ region was first reported in ref. [35]. This indicates that the $\Lambda(1405)$ resonance is not a single state but is instead a superposition of two eigenstates. The two-pole structure has a significant impact on hadron spectroscopy since it is related to the number of eigenstates in this sector. In general, a resonance state can have different coupling strengths to various channels. It was shown in ref. [31] that the high-mass pole of the $\Lambda(1405)$ strongly couples to $\bar{K}N$ and the low-mass pole has a large coupling to $\pi\Sigma$, as expected from their origin in the isospin basis.

To test the stability of the chiral dynamics model, an alternative fit is performed using a Flatté-like formula [36] in place of the chiral dynamics model. The Flatté-like formula is

Resonance	Mass (MeV/ c^2)	Width (MeV)	FF (%)
$\Lambda(1405)$	3.0 ± 0.3
$\Lambda(1520)$	1519.9 ± 1.6	20.6 ± 1.9	1.3 ± 0.4
$\Lambda(1600)$	1570.5 ± 4.6	228.1 ± 11.9	28.5 ± 1.5
$\Lambda(1670)$	1667.5 ± 2.3	30.2 ± 4.2	2.5 ± 0.6
$\Lambda(1690)$	1691.1 ± 4.4	72.3 ± 4.7	3.4 ± 0.7
$\Lambda(1800)$	1800.9 ± 13.3	208.8 ± 14.5	4.0 ± 1.0
$\Lambda(1890)$	1897.2 ± 9.6	149.2 ± 13.5	2.9 ± 0.6
$\Lambda(2325)$	2306.5 ± 6.3	227.1 ± 12.2	15.9 ± 1.2
$\Sigma(1385)$	1388.2 ± 1.9	60.5 ± 3.6	9.2 ± 0.7
$\Sigma(1660)$	1643.2 ± 4.5	221.3 ± 13.1	25.8 ± 2.0
$\Sigma(1670)$	1679.7 ± 3.4	87.0 ± 6.4	10.0 ± 1.5
$\Sigma(1750)$	1714.9 ± 4.2	97.2 ± 9.8	10.2 ± 1.5
$\Sigma(1910)$	1912.1 ± 10.6	225.1 ± 24.5	1.5 ± 0.6

Table 1: The resonant parameters and fitted fractions for each component, where the uncertainties are statistical only. The ellipses indicate that the parameter is not measured.

defined as

$$R(m) = \frac{1}{m_0^2 - m^2 - im_0[\sum_i g_i \frac{q_i}{m} \times \frac{m_0}{|q_{i0}|} \times \frac{|q_i|^{2l_i}}{|q_{i0}|^{2l_i}} B_{l_i}^{\prime 2}(|q_i|, |q_{i0}|, d)]}, \quad (6.9)$$

where

$$q_i = \begin{cases} \frac{\sqrt{(m^2 - (m_{i,1} + m_{i,2})^2)(m^2 - (m_{i,1} - m_{i,2})^2)}}{2m} & (m^2 - (m_{i,1} + m_{i,2})^2)(m^2 - (m_{i,1} - m_{i,2})^2) \geq 0, \\ i\frac{\sqrt{|(m^2 - (m_{i,1} + m_{i,2})^2)(m^2 - (m_{i,1} - m_{i,2})^2)|}}{2m} & (m^2 - (m_{i,1} + m_{i,2})^2)(m^2 - (m_{i,1} - m_{i,2})^2) < 0. \end{cases} \quad (6.10)$$

Here, m_0 is the mass of the resonance, $m_{i,1}$ and $m_{i,2}$ are the masses of the decay particles for the i -th channel, g_i is the partial width, l_i is the orbital angular momentum, and $B_{l_i}^{\prime 2}$ is the barrier factor. For the $\Lambda(1405)$, m_0 is fixed to be 1405.1 MeV/ c^2 , as quoted from the PDG [16], and g_i is a free parameter. The decay of the $\Lambda(1405)$ includes both $\pi\Sigma$ and $\bar{K}N$ channels, $m_{i,1}$ and $m_{i,2}$ are quoted from the PDG [16], and the l_i are all fixed to be 0. The statistical significance and fitted fraction of the $\Lambda(1405)$ are 11.1σ and $(3.0 \pm 0.3)\%$ in nominal fit, and 11.2σ and $(6.7 \pm 0.9)\%$ in alternative fit with the Flatté-like formula. Due to the similar statistical significance of the $\Lambda(1405)$ with the two different parameterization and the chiral dynamics model is well established in the literature, the parameterization of the chiral dynamics is found to be reasonable and is used in the nominal PWA fit.

A one-star resonance, the $\Lambda(2325)$, is also added to the nominal fit. It was first reported in ref. [37] with $J^P = 3/2^-$. A check on the spin-parity of the $\Lambda(2325)$ has been performed. A comparison of the statistical significance with the different spin-parity hypotheses ($1/2^-$, $1/2^+$, $3/2^-$ and $3/2^+$) is shown in table 2. The statistical significance is calculated based

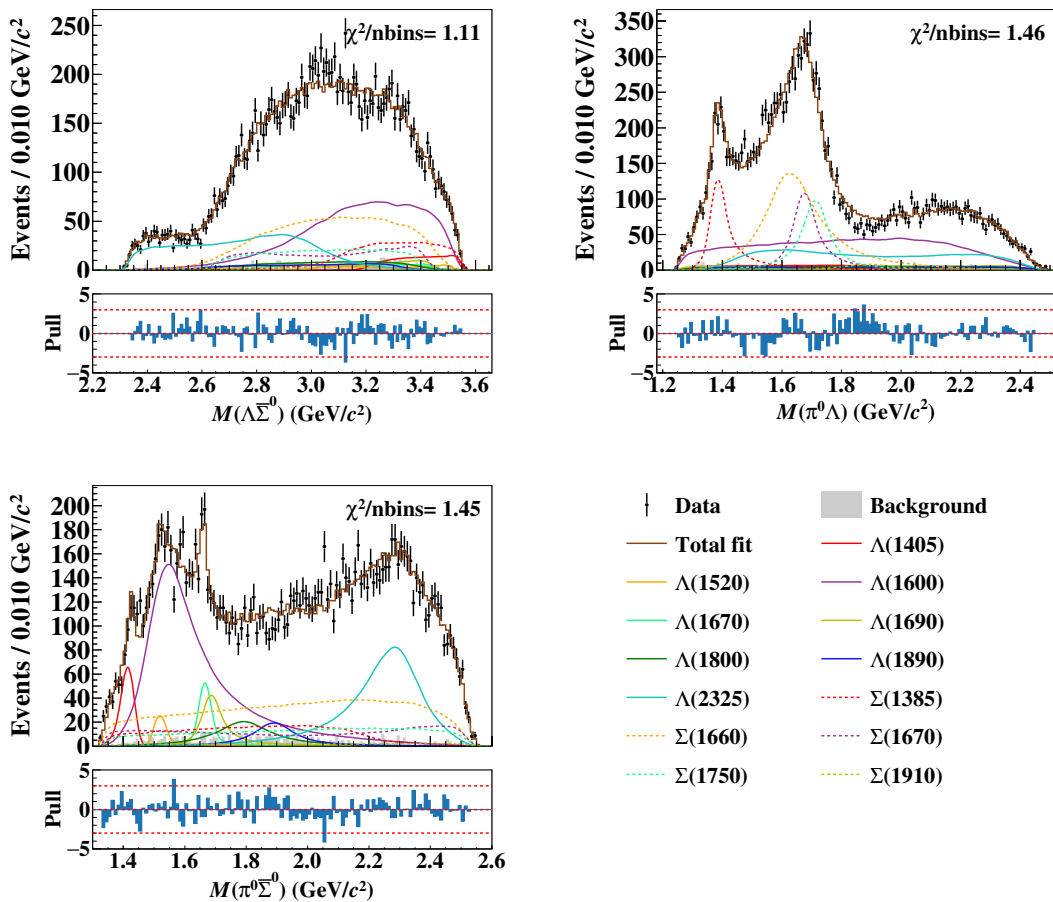


Figure 4: The distributions of $M(\Lambda\bar{\Sigma}^0)$, $M(\pi^0\Lambda)$, and $M(\pi^0\bar{\Sigma}^0)$. The legend is shown in the bottom right.

J^P	ΔN_{LL}	ΔN_{dof}	Significance (σ)
$1/2^-$	188.0	6	18.7
$1/2^+$	186.8	6	18.6
$3/2^-$	208.3	8	19.5
$3/2^+$	198.8	8	19.1

Table 2: Comparison of the different quantum numbers for the spin-parity of the $\Lambda(2325)$.

on the change of the N_{LL} values with and without including the component, by taking into account the change of the number of degrees of freedom. Based on the comparison, the spin-parity of the $\Lambda(2325)$ is most likely $J^P = 3/2^-$, which is consistent with the PDG [16].

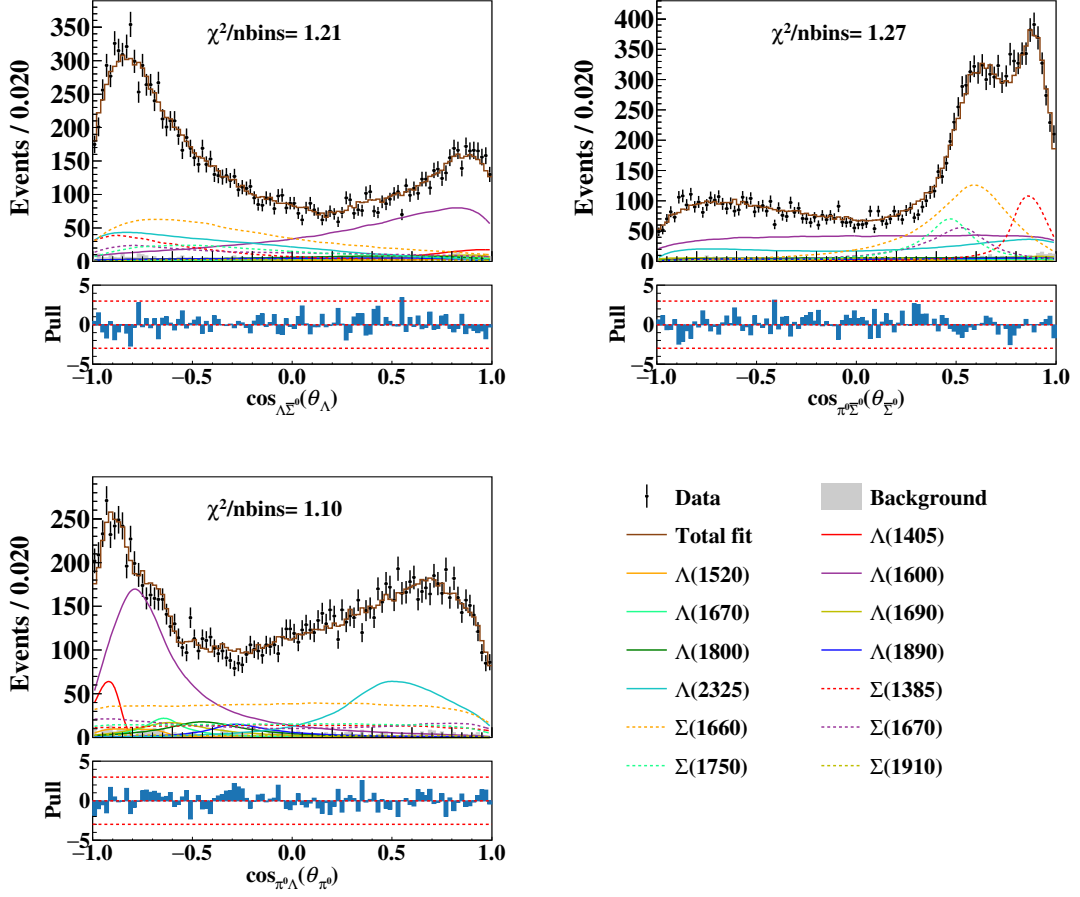


Figure 5: The distributions of $\cos_{\Lambda\bar{\Sigma}^0}(\theta_{\Lambda})$, $\cos_{\pi^0\bar{\Sigma}^0}(\theta_{\bar{\Sigma}^0})$, and $\cos_{\pi^0\Lambda}(\theta_{\pi^0})$. The legend is shown in the bottom right.

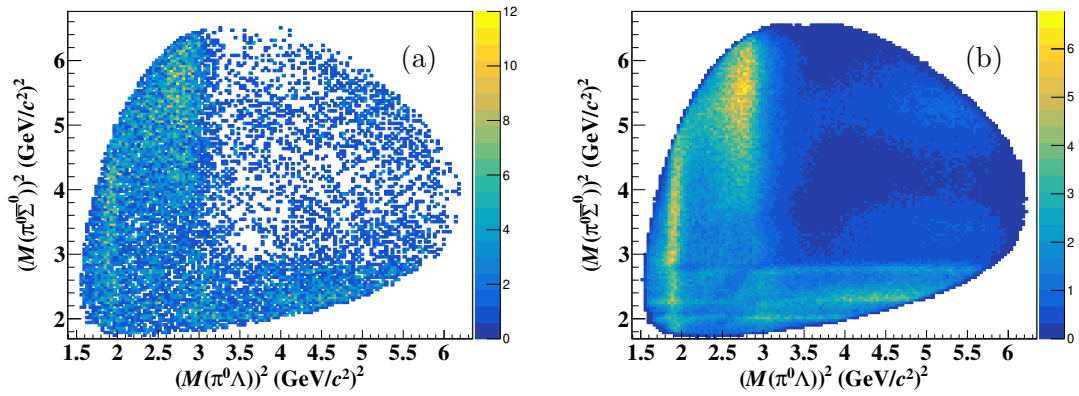


Figure 6: The Dalitz plots of $(M(\pi^0\Lambda))^2$ versus $(M(\pi^0\bar{\Sigma}^0))^2$ of (a) data and (b) the PWA fit result.

Component	N^{obs}	ϵ (%)	\mathcal{B} ($\times 10^{-5}$)
$\psi(3686) \rightarrow \Lambda(1405)\bar{\Lambda}$	429.3 ± 47.5	10.3	0.38 ± 0.04
$\psi(3686) \rightarrow \Lambda(1520)\bar{\Lambda}$	192.2 ± 51.9	8.6	0.20 ± 0.05
$\psi(3686) \rightarrow \Lambda(1600)\bar{\Lambda}$	4061.4 ± 223.0	9.5	3.92 ± 0.22
$\psi(3686) \rightarrow \Lambda(1670)\bar{\Lambda}$	355.4 ± 79.7	9.8	0.33 ± 0.07
$\psi(3686) \rightarrow \Lambda(1690)\bar{\Lambda}$	486.3 ± 93.7	9.6	0.47 ± 0.09
$\psi(3686) \rightarrow \Lambda(1800)\bar{\Lambda}$	565.8 ± 141.8	11.0	0.47 ± 0.12
$\psi(3686) \rightarrow \Lambda(1890)\bar{\Lambda}$	410.3 ± 91.2	9.8	0.38 ± 0.09
$\psi(3686) \rightarrow \Lambda(2325)\bar{\Lambda}$	2270.7 ± 175.4	7.6	2.72 ± 0.21
$\psi(3686) \rightarrow \Sigma(1385)^0\bar{\Sigma}^0$	1312.2 ± 102.8	8.9	1.35 ± 0.11
$\psi(3686) \rightarrow \Sigma(1660)^0\bar{\Sigma}^0$	3680.6 ± 291.7	9.5	3.56 ± 0.28
$\psi(3686) \rightarrow \Sigma(1670)^0\bar{\Sigma}^0$	1425.3 ± 220.3	9.5	1.37 ± 0.21
$\psi(3686) \rightarrow \Sigma(1750)^0\bar{\Sigma}^0$	1458.8 ± 218.4	10.9	1.22 ± 0.18
$\psi(3686) \rightarrow \Sigma(1910)^0\bar{\Sigma}^0$	217.0 ± 92.2	9.6	0.21 ± 0.09

Table 3: The signal yields in data, the detection efficiencies, and the branching fractions for each component. The uncertainties of the signal yields and branching fractions are statistical only.

6.3 Branching fractions

The branching fractions of the intermediate states are determined by

$$\mathcal{B} = \frac{N^{\text{obs}}}{N_{\psi(3686)} \cdot \mathcal{B}^2(\Lambda \rightarrow p\pi^-) \cdot \mathcal{B}(\pi^0 \rightarrow \gamma\gamma) \cdot \mathcal{B}(\Sigma^0 \rightarrow \gamma\Lambda) \cdot \epsilon}, \quad (6.11)$$

where N^{obs} is the number of signal events in data, $N_{\psi(3686)}$ is the number of $\psi(3686)$ events in data determined with inclusive hadronic events, ϵ is the detection efficiency obtained from the signal MC sample generated with the PWA results, and $\mathcal{B}(\Lambda \rightarrow p\pi^-)$, $\mathcal{B}(\pi^0 \rightarrow \gamma\gamma)$, and $\mathcal{B}(\Sigma^0 \rightarrow \gamma\Lambda)$ are the corresponding branching fractions quoted from the PDG [16]. The obtained branching fractions are summarized in table 3.

7 Systematic uncertainties

7.1 Systematic uncertainties on branching fraction

The systematic uncertainties on the branching fraction measurement mainly originate from photon and $\Lambda(\bar{\Lambda})$ reconstruction, the 4C kinematic fit, selection of the π^0 signal region, the signal shape, the background shape, the MC model, the quoted branching fractions for intermediate states, and the total number of $\psi(3686)$ events. All sources are listed in table 4 and are discussed in detail below. Assuming all sources are independent, the total systematic uncertainty is determined by adding them in quadrature.

1. The efficiency of the $\Lambda(\bar{\Lambda})$ reconstruction, incorporating both the MDC tracking and the $\Lambda(\bar{\Lambda})$ mass window requirement, is studied using a control sample of $\psi(3686) \rightarrow$

$\Lambda\bar{\Lambda}$ decays, and a correction factor of 0.980 ± 0.011 [38] is applied to the detection efficiencies obtained from MC simulation. After the efficiency correction we take 1.1% as the systematic uncertainty due to the $\Lambda(\bar{\Lambda})$ reconstruction.

2. For photons directly detected by the EMC, the detection efficiency is studied using a control sample of $e^+e^- \rightarrow \gamma_{\text{ISR}}\mu^+\mu^-$, where ISR stands for initial state radiation. The systematic uncertainty, defined as the relative difference in efficiencies between data and MC simulation, is observed to be up to 0.5% per photon in both the barrel and end-cap regions. Thus, the total systematic uncertainty of the three photons is 1.5%.
3. The uncertainty associated with the 4C kinematic fit is due to the inconsistency between data and MC simulation. This difference has been reduced by correcting the track helix parameters in the MC simulation, with parameters taken from refs. [39, 40]. Following the method described in ref. [41], the difference between the corrected and uncorrected efficiencies, 1.4%, is assigned as the systematic uncertainty due to the 4C kinematic fit.
4. The uncertainty due to the π^0 signal region is evaluated by varying the nominal signal region by $\pm 1\sigma$ of its mass resolution, i.e., $\pm 6 \text{ MeV}/c^2$. The maximum difference in branching fraction, 0.7%, is assigned as the systematic uncertainty.
5. In order to evaluate the systematic uncertainty due to the signal shape, an alternative fit is performed to determine the number of signal events. The simulated signal shape is replaced with a Crystal-ball function convolved with a Gaussian function, and the fit range is changed by $\pm 10 \text{ MeV}$. The maximum difference in branching fraction, 2.5%, is assigned as the corresponding systematic uncertainty.
6. To estimate the uncertainty of the non-peaking and mis-combination background shape, we perform an alternative fit by replacing the first-order with a second-order Chebychev polynomial function. The difference in branching fraction is found to be 0.3%, which is assigned as the systematic uncertainty due to the background shape.
7. The uncertainty due to the MC model is evaluated by comparing the efficiencies between the nominal and alternative models. The efficiency difference between different models is taken as the systematic uncertainty.
8. The uncertainties from the quoted branching fractions of the intermediate decays of $\Lambda \rightarrow p\pi^-$ and $\pi^0 \rightarrow \gamma\gamma$ are taken from the PDG [16]. Since the branching fraction of $\Sigma^0 \rightarrow \gamma\Lambda$ is equal to 100% with no uncertainty, it is not considered in the systematic uncertainty.
9. The total number of $\psi(3686)$ events in data is determined using inclusive hadronic decays. Its uncertainty, 0.5% [3], is taken as a systematic uncertainty.

Source	Uncertainty (%)
$\Lambda(\bar{\Lambda})$ reconstruction	2.2
Photon reconstruction	1.5
Kinematic fit	1.4
π^0 signal region	0.7
Signal shape	2.5
Background shape	0.4
MC model	1.1
$\mathcal{B}(\Lambda \rightarrow p\pi)$	1.6
$\mathcal{B}(\pi^0 \rightarrow \gamma\gamma)$	0.02
Total number of $\psi(3686)$ events	0.5
Total	4.5

Table 4: The systematic uncertainties for the branching fraction.

7.2 Systematic uncertainties on partial wave analysis

The systematic uncertainties on the PWA mainly originate from other possible components, the background estimation, the parameterization of the $\Lambda(1405)$, and the radius of the Blatt-Weisskopf barrier factor. All sources are listed in tables 5, 6, and 7, and discussed in detail below. Assuming all sources are independent, the total systematic uncertainty is determined by adding them in quadrature.

1. To evaluate the effect on the PWA results from other possible components, the PWA is re-performed by adding extra resonances ($\Lambda(1810)$, $\Lambda(1820)$, $\Lambda(1830)$, $\Sigma(1775)$, $\Sigma(1915)$, $\rho_3(2250)$, $\rho_5(2350)$) one at a time. The largest changes of the masses, widths, and fitted fractions of resonances are taken as the systematic uncertainties.
2. The uncertainty due to the background estimation is evaluated by varying the yields of the $\Sigma^0/\bar{\Sigma}^0$ sideband and the continuum production within $\pm 1\sigma$ of its statistical uncertainty. The largest difference for each result is taken as the systematic uncertainty.
3. The uncertainty due to the $\Lambda(1405)$ parameterization is evaluated by replacing the nominal formula by the Flatté-like formula. The differences of the masses, widths, and fitted fractions of resonances are taken as the systematic uncertainties.
4. In the PWA, the radius d in the Blatt-Weisskopf barrier factors [28] is chosen as $d = 0.73 \text{ fm} \approx 3.7 \text{ GeV}^{-1}$ following ref. [30]. The associated systematic uncertainty is evaluated by varying the radius d in the range $d \in [1, 5] \text{ GeV}^{-1}$ [16]. The largest differences of the masses, widths, and fitted fractions of resonances are taken as the systematic uncertainties.

Resonance	EX-RES	BKG	PARAM	BW-BF	Total
$\Lambda(1520)$	4.1	1.7	0.1	0.5	4.5
$\Lambda(1600)$	8.9	5.0	2.8	4.3	11.5
$\Lambda(1670)$	1.2	2.2	0.6	0.8	2.7
$\Lambda(1690)$	7.8	8.9	2.2	2.2	12.2
$\Lambda(1800)$	2.2	2.1	8.6	8.5	12.5
$\Lambda(1890)$	1.9	1.8	2.1	4.9	5.9
$\Lambda(2325)$	10.4	8.5	1.9	8.5	16.0
$\Sigma(1385)$	1.5	1.5	0.3	2.1	3.0
$\Sigma(1660)$	4.7	4.4	2.6	0.5	7.0
$\Sigma(1670)$	1.8	1.7	3.1	0.5	4.0
$\Sigma(1750)$	6.0	1.6	1.0	3.5	7.2
$\Sigma(1910)$	23.7	4.2	9.8	21.0	33.4

Table 5: The systematic uncertainty sources for the masses in units of MeV/c^2 . The EX-RES is extra resonances, the BKG is background, the PARAM is parameterization of the $\Lambda(1405)$, and the BW-BF is the Blatt-Weisskopf barrier factor.

Resonance	EX-RES	BKG	PARAM	BW-BF	Total
$\Lambda(1520)$	0.2	0.2	0.3	0.4	0.6
$\Lambda(1600)$	28.7	8.2	8.7	7.8	32.1
$\Lambda(1670)$	5.1	4.8	0.1	2.6	7.4
$\Lambda(1690)$	9.7	11.6	1.7	0.9	15.2
$\Lambda(1800)$	36.1	3.0	3.8	9.2	37.6
$\Lambda(1890)$	2.0	1.9	1.7	1.6	3.7
$\Lambda(2325)$	47.5	2.2	1.7	4.1	47.7
$\Sigma(1385)$	6.0	0.6	0.9	4.0	7.3
$\Sigma(1660)$	35.3	3.5	0.0	10.4	37.0
$\Sigma(1670)$	4.4	4.2	3.7	2.9	7.7
$\Sigma(1750)$	8.5	2.6	2.5	2.2	9.5
$\Sigma(1910)$	36.6	17.4	5.4	10.3	42.1

Table 6: The systematic uncertainty sources for the widths in units of MeV. The EX-RES is extra resonances, the BKG is background, the PARAM is parameterization of the $\Lambda(1405)$, and the BW-BF is the Blatt-Weisskopf barrier factor.

Resonance	BF	EX-RES	BKG	PARAM	BW-BF	Total
$\Lambda(1405)$	4.5	21.0	6.7	11.8	0.8	25.4
$\Lambda(1520)$	4.5	19.9	6.3	12.9	8.3	26.2
$\Lambda(1600)$	4.5	21.2	3.4	15.3	4.5	27.1
$\Lambda(1670)$	4.5	21.9	12.1	0.7	5.7	26.0
$\Lambda(1690)$	4.5	14.3	5.7	4.9	5.9	17.8
$\Lambda(1800)$	4.5	24.2	11.1	3.4	8.3	28.5
$\Lambda(1890)$	4.5	8.5	11.1	2.3	7.4	16.6
$\Lambda(2325)$	4.5	2.5	4.7	2.4	3.2	8.0
$\Sigma(1385)$	4.5	11.7	3.4	4.5	4.9	14.6
$\Sigma(1660)$	4.5	13.6	5.5	5.3	4.2	16.8
$\Sigma(1670)$	4.5	17.5	6.7	11.9	4.9	23.2
$\Sigma(1750)$	4.5	19.4	3.8	6.4	8.9	23.0
$\Sigma(1910)$	4.5	22.0	2.9	9.9	9.9	26.6

Table 7: The systematic uncertainty sources for the fitted fractions in percentage. The BF is uncertainty from branching fraction measurements, the EX-RES is extra resonances, the BKG is background, the PARAM is parameterization of the $\Lambda(1405)$, and the BW-BF is the Blatt-Weisskopf barrier factor.

8 Summary

Based on a sample of $(2712.4 \pm 14.3) \times 10^6$ $\psi(3686)$ events [3] collected with the BESIII detector, a PWA of $\psi(3686) \rightarrow \Lambda \bar{\Sigma}^0 \pi^0$ is performed for the first time to investigate possible Λ^* and Σ^* states. The measured masses, widths, and product branching fractions for each component are summarized in table 8. In addition to the well established Λ^* and Σ^* states, including the $\Lambda(1405)$, $\Lambda(1520)$, $\Lambda(1600)$, $\Lambda(1670)$, $\Lambda(1690)$, $\Lambda(1800)$, $\Lambda(1890)$, $\Sigma(1385)$, $\Sigma(1660)$, $\Sigma(1670)$, $\Sigma(1750)$, and $\Sigma(1910)$, the PWA results indicate that the $\Lambda(2325)$ is necessary to better describe data. It is found that both the chiral dynamics model and the Flatté-like formula for the parameterization of the $\Lambda(1405)$ can describe the data well. Due to the low statistics of the data, the two models are not distinguishable. Although the $\Lambda(2325)$ is a one-star state in the PDG [16], it is also one of the dominant contributions in $\psi(3686) \rightarrow \Lambda \bar{\Sigma}^0 \pi^0$, which provides further proof of the existence of the $\Lambda(2325)$. We also perform a check on its spin-parity and find that its spin-parity favors $J^P = 3/2^-$, which is consistent with that in the PDG [16]. In addition, the branching fraction of $\psi(3686) \rightarrow \Lambda \bar{\Sigma}^0 \pi^0 + c.c.$ is measured to be $(1.544 \pm 0.013 \pm 0.069) \times 10^{-4}$ for the first time.

Acknowledgments

The BESIII Collaboration thanks the staff of BEPCII and the IHEP computing center for their strong support. This work is supported in part by National Key R&D Program of China under Contracts Nos. 2020YFA0406300, 2020YFA0406400, 2023YFA1606000;

Resonance	Mass (MeV/ c^2)	Width (MeV)	\mathcal{B} ($\times 10^{-5}$)
$\Lambda(1405)$	$0.38 \pm 0.04 \pm 0.10$
$\Lambda(1520)$	$1519.9 \pm 1.6 \pm 4.5$	$20.6 \pm 1.9 \pm 0.5$	$0.20 \pm 0.05 \pm 0.05$
$\Lambda(1600)$	$1570.5 \pm 4.6 \pm 11.4$	$228.1 \pm 11.9 \pm 33.8$	$3.92 \pm 0.22 \pm 1.06$
$\Lambda(1670)$	$1667.5 \pm 2.3 \pm 2.7$	$30.2 \pm 4.2 \pm 7.3$	$0.33 \pm 0.07 \pm 0.09$
$\Lambda(1690)$	$1691.1 \pm 4.4 \pm 12.2$	$72.3 \pm 4.7 \pm 15.4$	$0.47 \pm 0.09 \pm 0.08$
$\Lambda(1800)$	$1800.9 \pm 13.3 \pm 12.4$	$208.8 \pm 14.5 \pm 36.6$	$0.47 \pm 0.12 \pm 0.13$
$\Lambda(1890)$	$1897.2 \pm 9.6 \pm 5.9$	$149.2 \pm 13.5 \pm 3.7$	$0.38 \pm 0.09 \pm 0.06$
$\Lambda(2325)$	$2306.5 \pm 6.3 \pm 16.0$	$227.1 \pm 12.2 \pm 47.8$	$2.72 \pm 0.21 \pm 0.22$
$\Sigma(1385)$	$1388.2 \pm 1.9 \pm 3.0$	$60.5 \pm 3.6 \pm 6.3$	$1.35 \pm 0.11 \pm 0.20$
$\Sigma(1660)$	$1643.2 \pm 4.5 \pm 6.9$	$221.3 \pm 13.1 \pm 41.0$	$3.56 \pm 0.28 \pm 0.60$
$\Sigma(1670)$	$1679.7 \pm 3.4 \pm 4.0$	$87.0 \pm 6.4 \pm 7.8$	$1.37 \pm 0.21 \pm 0.32$
$\Sigma(1750)$	$1714.9 \pm 4.2 \pm 7.2$	$97.2 \pm 9.8 \pm 9.3$	$1.22 \pm 0.18 \pm 0.28$
$\Sigma(1910)$	$1912.1 \pm 10.6 \pm 33.4$	$225.1 \pm 24.5 \pm 43.3$	$0.21 \pm 0.09 \pm 0.05$

Table 8: The masses, widths, and product branching fractions of each component in the nominal PWA fit. The first uncertainties are statistical and the second systematic.

National Natural Science Foundation of China (NSFC) under Contracts Nos. 12075107, 12247101, 12175244, 11635010, 11735014, 11935015, 11935016, 11935018, 12025502, 12035009, 12035013, 12061131003, 12192260, 12192261, 12192262, 12192263, 12192264, 12192265, 12221005, 12225509, 12235017, 12361141819; the 111 Project under Grant No. B20063; the Chinese Academy of Sciences (CAS) Large-Scale Scientific Facility Program; the CAS Center for Excellence in Particle Physics (CCEPP); Joint Large-Scale Scientific Facility Funds of the NSFC and CAS under Contract Nos. U2032110, U1832207; 100 Talents Program of CAS; The Institute of Nuclear and Particle Physics (INPAC) and Shanghai Key Laboratory for Particle Physics and Cosmology; German Research Foundation DFG under Contracts Nos. 455635585, FOR5327, GRK 2149; Istituto Nazionale di Fisica Nucleare, Italy; Ministry of Development of Turkey under Contract No. DPT2006K-120470; National Research Foundation of Korea under Contract No. NRF-2022R1A2C1092335; National Science and Technology fund of Mongolia; National Science Research and Innovation Fund (NSRF) via the Program Management Unit for Human Resources & Institutional Development, Research and Innovation of Thailand under Contract No. B16F640076; Polish National Science Centre under Contract No. 2019/35/O/ST2/02907; The Swedish Research Council; U. S. Department of Energy under Contract No. DE-FG02-05ER41374

References

- [1] R. G. Edwards, J. J. Dudek, D. G. Richards and S. J. Wallace, *Excited state baryon spectroscopy from lattice QCD*, *Phys. Rev. D* **84** (2011) 074508 [arXiv:1104.5152] [INSPIRE].
- [2] E. Klempt and J. M. Richard, *Baryon spectroscopy*, *Rev. Mod. Phys.* **82** (2010) 1095-1153 [arXiv:0901.2055] [INSPIRE].

- [3] BESIII collaboration, *Determination of the number of $\psi(3686)$ events taken at BESIII*, [[arXiv:2403.06766](#)] [[INSPIRE](#)].
- [4] BESIII collaboration, *Design and Construction of the BESIII Detector*, *Nucl. Instrum. Meth. A* **614** (2010) 345-399 [[arXiv:0911.4960](#)] [[INSPIRE](#)].
- [5] C. Yu et al., *BEPCh Performance and Beam Dynamics Studies on Luminosity*, in the proceedings of the 7th *International Particle Accelerator Conference*, (2016), p. TUYA01 [[DOI:10.18429/JACoW-IPAC2016-TUYA01](#)] [[INSPIRE](#)].
- [6] BESIII collaboration, *Future Physics Programme of BESIII*, *Chin. Phys. C* **44** (2020) 040001 [[arXiv:1912.05983](#)] [[INSPIRE](#)].
- [7] J.-W. Zhang et al., *Suppression of top-up injection backgrounds with offline event filter in the BESIII experiment*, *Radiat. Detect. Technol. Methods* **6** (2022) 289-293 [[INSPIRE](#)].
- [8] X. Li et al., *Study of MRPC technology for BESIII endcap-TOF upgrade*, *Radiat. Detect. Technol. Methods* **1** (2017) 13 [[INSPIRE](#)].
- [9] Y.-X. Guo et al., *The study of time calibration for upgraded end cap TOF of BESIII*, *Radiat. Detect. Technol. Methods* **1** (2017) 15 [[INSPIRE](#)].
- [10] P. Cao et al., *Design and construction of the new BESIII endcap Time-of-Flight system with MRPC Technology*, *Nucl. Instrum. Meth. A* **953** (2020) 163053 [[INSPIRE](#)].
- [11] GEANT4 collaboration, *GEANT4—a simulation toolkit*, *Nucl. Instrum. Meth. A* **506** (2003) 250-303 [[INSPIRE](#)].
- [12] S. Jadach, B. F. L. Ward and Z. Was, *Coherent exclusive exponentiation for precision Monte Carlo calculations*, *Phys. Rev. D* **63** (2001) 113009 [[hep-ph/0006359](#)] [[INSPIRE](#)].
- [13] S. Jadach, B. F. L. Ward and Z. Was, *The Precision Monte Carlo event generator KK for two fermion final states in e^+e^- collisions*, *Comput. Phys. Commun.* **130** (2000) 260-325 [[hep-ph/9912214](#)] [[INSPIRE](#)].
- [14] D. J. Lange, *The EvtGen particle decay simulation package*, *Nucl. Instrum. Meth. A* **462** (2001) 152-155 [[INSPIRE](#)].
- [15] R.-G. Ping, *Event generators at BESIII*, *Chin. Phys. C* **32** (2008) 599 [[INSPIRE](#)].
- [16] PARTICLE DATA GROUP collaboration, *Review of Particle Physics*, *PTEP* **2022** (2022) 083C01 [[INSPIRE](#)].
- [17] J. C. Chen, G. S. Huang, X. R. Qi, D. H. Zhang and Y. S. Zhu, *Event generator for J/ψ and $\psi(3686)$ decay*, *Phys. Rev. D* **62** (2000) 034003 [[INSPIRE](#)].
- [18] R.-L. Yang, R.-G. Ping and H. Chen, *Tuning and Validation of the Lundcharm Model with J/ψ Decays*, *Chin. Phys. Lett.* **31** (2014) 061301 [[INSPIRE](#)].
- [19] E. Richter-Was, *QED bremsstrahlung in semileptonic B and leptonic tau decays*, *Phys. Lett. B* **303** (1993) 163-169 [[INSPIRE](#)].
- [20] M. Xu et al., *Decay vertex reconstruction and 3-dimensional lifetime determination at BESIII*, *Chin. Phys. C* **33** (2009) 428-435 [[INSPIRE](#)].
- [21] X. Zhou, S. Du, G. Li and C. Shen, *TopoAna: A generic tool for the event type analysis of inclusive Monte-Carlo samples in high energy physics experiments*, *Comput. Phys. Commun.* **258** (2021) 107540 [[arXiv:2001.04016](#)] [[INSPIRE](#)].

- [22] BESIII collaboration, *Measurement of the integrated luminosities of the data taken by BESIII at $\sqrt{s} = 3.650$ and 3.773 GeV*, *Chin. Phys. C* **37** (2013) 123001 [arXiv:1307.2022] [INSPIRE].
- [23] BESIII collaboration, *Measurement of the $e^+e^- \rightarrow \pi^+\pi^-$ cross section between 600 and 900 MeV using initial state radiation*, *Phys. Lett. B* **753** (2016) 629-638 [Erratum: *Phys. Lett. B* **812** (2021) 135982] [arXiv:1507.08188] [INSPIRE].
- [24] BESIII collaboration, *Measurement of the integrated luminosity of the data collected at 3.773 GeV by BESIII from 2021 to 2024*, [arXiv:2406.05827] [INSPIRE].
- [25] D. M. Asner et al., *Physics at BES-III*, *Int. J. Mod. Phys. A* **24**, S1-794 (2009) [arXiv:0809.1869] [INSPIRE].
- [26] Y. Jiang et al., *Open-source framework TF-PWA package*, GitHub link: <https://github.com/jiangyi15/tf-pwa> (2020).
- [27] S. U. Chung, *A General formulation of covariant helicity coupling amplitudes*, *Phys. Rev. D* **57** (1998) 431-442 [INSPIRE].
- [28] S. U. Chung, *Helicity coupling amplitudes in tensor formalism*, *Phys. Rev. D* **48** (1993) 1225-1239 [Erratum: *Phys. Rev. D* **56** (1997) 4419] [INSPIRE].
- [29] M. Wang, Y. Jiang, Y. Liu, W. Qian, X. Lyu and L. Zhang, *A novel method to test particle ordering and final state alignment in helicity formalism*, *Chin. Phys. C* **45** (2021) 063103 [arXiv:2012.03699] [INSPIRE].
- [30] BESIII collaboration, *Partial wave analysis of $\psi(3686) \rightarrow K^+K^-\eta$* , *Phys. Rev. D* **101** (2020) 032008 [arXiv:1912.08566] [INSPIRE].
- [31] D. Jido, J. A. Oller, E. Oset, A. Ramos and U. G. Meissner, *Chiral dynamics of the two $\Lambda(1405)$ states*, *Nucl. Phys. A* **725** (2003) 181-200 [nucl-th/0303062] [INSPIRE].
- [32] E. Oset and A. Ramos, *Nonperturbative chiral approach to s -wave $\bar{K}N$ interactions*, *Nucl. Phys. A* **635** (1998) 99-120 [nucl-th/9711022] [INSPIRE].
- [33] E. Oset, A. Ramos and C. Bennhold, *Low lying $S = -1$ excited baryons and chiral symmetry*, *Phys. Lett. B* **527** (2002) 99-105 [nucl-th/0109006] [INSPIRE].
- [34] BESIII collaboration, *Partial wave analysis of the charmed baryon hadronic decay $\Lambda_c^+ \rightarrow \Lambda\pi^+\pi^0$* , *JHEP* **12** (2022) 033 [arXiv:2209.08464] [INSPIRE].
- [35] J. A. Oller and U. G. Meissner, *Chiral dynamics in the presence of bound states: Kaon nucleon interactions revisited*, *Phys. Lett. B* **500** (2001) 263-272 [hep-ph/0011146] [INSPIRE].
- [36] S. U. Chung, J. Brose, R. Hackmann, E. Klempt, S. Spanier and C. Strassburger, *Partial wave analysis in K matrix formalism*, *Annalen Phys.* **4** (1995) 404-430 [INSPIRE].
- [37] B. Baccari et al., *New Data on $K-p \rightarrow \omega$ Lambda from 1.934 – GeV/c to 2.516 – GeV/c and Partial Wave Analyses from Threshold U_p to 2436 – MeV CMS Energy*, *Nuovo Cim. A* **41** (1977) 96 [INSPIRE].
- [38] BESIII collaboration, *Study of J/ψ and $\psi(3686)$ decay to $\Lambda\bar{\Lambda}$ and $\Sigma^0\bar{\Sigma}^0$ final states*, *Phys. Rev. D* **95** (2017) 052003 [arXiv:1701.07191] [INSPIRE].
- [39] BESIII collaboration, *Search for $\eta_c(2S)h_c \rightarrow p\bar{p}$ decays and measurements of the $\chi_{cJ} \rightarrow p\bar{p}$ branching fractions*, *Phys. Rev. D* **88** (2013) 112001 [arXiv:1310.6099] [INSPIRE].
- [40] BESIII collaboration, *Cross section measurements of $e^+e^- \rightarrow \omega\chi_{c0}$ form $\sqrt{s} = 4.178$ to 4.278 GeV*, *Phys. Rev. D* **99** (2019) 091103 [arXiv:1903.02359] [INSPIRE].

- [41] BESIII collaboration, *Search for hadronic transition $\chi_{cJ} \rightarrow \eta_c \pi^+ \pi^-$ and observation of $\chi_{cJ} \rightarrow K \bar{K} \pi \pi$* , *Phys. Rev. D* **87** (2013) 012002 [[arXiv:1208.4805](#)] [[INSPIRE](#)].

The BESIII collaboration

M. Ablikim¹, M. N. Achasov^{4,c}, P. Adlarson⁷⁶, O. Afedulidis³, X. C. Ai⁸¹, R. Aliberti³⁵, A. Amoroso^{75A,75C}, Q. An^{72,58,a}, Y. Bai⁵⁷, O. Bakina³⁶, I. Balossino^{29A}, Y. Ban^{46,h}, H.-R. Bao⁶⁴, V. Batozskaya^{1,44}, K. Begzsuren³², N. Berger³⁵, M. Berlowski⁴⁴, M. Bertani^{28A}, D. Bettoni^{29A}, F. Bianchi^{75A,75C}, E. Bianco^{75A,75C}, A. Bortone^{75A,75C}, I. Boyko³⁶, R. A. Briere⁵, A. Brueggemann⁶⁹, H. Cai⁷⁷, X. Cai^{1,58}, A. Calcaterra^{28A}, G. F. Cao^{1,64}, N. Cao^{1,64}, S. A. Cetin^{62A}, X. Y. Chai^{46,h}, J. F. Chang^{1,58}, G. R. Che⁴³, G. Chelkov^{36,b}, C. Chen⁴³, C. H. Chen⁹, Chao Chen⁵⁵, G. Chen¹, H. S. Chen^{1,64}, H. Y. Chen²⁰, M. L. Chen^{1,58,64}, S. J. Chen⁴², S. L. Chen⁴⁵, S. M. Chen⁶¹, T. Chen^{1,64}, X. R. Chen^{31,64}, X. T. Chen^{1,64}, Y. B. Chen^{1,58}, Y. Q. Chen³⁴, Z. J. Chen^{25,i}, Z. Y. Chen^{1,64}, S. K. Choi¹⁰, G. Cibinetto^{29A}, F. Cossio^{75C}, J. J. Cui⁵⁰, H. L. Dai^{1,58}, J. P. Dai⁷⁹, A. Dbeyssi¹⁸, R. E. de Boer³, D. Dedovich³⁶, C. Q. Deng⁷³, Z. Y. Deng¹, A. Denig³⁵, I. Denysenko³⁶, M. Destefanis^{75A,75C}, F. De Mori^{75A,75C}, B. Ding^{67,1}, X. X. Ding^{46,h}, Y. Ding³⁴, Y. Ding⁴⁰, J. Dong^{1,58}, L. Y. Dong^{1,64}, M. Y. Dong^{1,58,64}, X. Dong⁷⁷, M. C. Du¹, S. X. Du⁸¹, Y. Y. Duan⁵⁵, Z. H. Duan⁴², P. Egorov^{36,b}, Y. H. Fan⁴⁵, J. Fang⁵⁹, J. Fang^{1,58}, S. S. Fang^{1,64}, W. X. Fang¹, Y. Fang¹, Y. Q. Fang^{1,58}, R. Farinelli^{29A}, L. Fava^{75B,75C}, F. Feldbauer³, G. Felici^{28A}, C. Q. Feng^{72,58}, J. H. Feng⁵⁹, Y. T. Feng^{72,58}, M. Fritsch³, C. D. Fu¹, J. L. Fu⁶⁴, Y. W. Fu^{1,64}, H. Gao⁶⁴, X. B. Gao⁴¹, Y. N. Gao^{46,h}, Yang Gao^{72,58}, S. Garbolino^{75C}, I. Garzia^{29A,29B}, L. Ge⁸¹, P. T. Ge¹⁹, Z. W. Ge⁴², C. Geng⁵⁹, E. M. Gersabeck⁶⁸, A. Gilman⁷⁰, K. Goetzen¹³, L. Gong⁴⁰, W. X. Gong^{1,58}, W. Gradl³⁵, S. Gramigna^{29A,29B}, M. Greco^{75A,75C}, M. H. Gu^{1,58}, Y. T. Gu¹⁵, C. Y. Guan^{1,64}, A. Q. Guo^{31,64}, L. B. Guo⁴¹, M. J. Guo⁵⁰, R. P. Guo⁴⁹, Y. P. Guo^{12,g}, A. Guskov^{36,b}, J. Gutierrez²⁷, K. L. Han⁶⁴, T. T. Han¹, F. Hanisch³, X. Q. Hao¹⁹, F. A. Harris⁶⁶, K. K. He⁵⁵, K. L. He^{1,64}, F. H. Heinsius³, C. H. Heinz³⁵, Y. K. Heng^{1,58,64}, C. Herold⁶⁰, T. Holtmann³, P. C. Hong³⁴, G. Y. Hou^{1,64}, X. T. Hou^{1,64}, Y. R. Hou⁶⁴, Z. L. Hou¹, B. Y. Hu⁵⁹, H. M. Hu^{1,64}, J. F. Hu^{56,j}, S. L. Hu^{12,g}, T. Hu^{1,58,64}, Y. Hu¹, G. S. Huang^{72,58}, K. X. Huang⁵⁹, L. Q. Huang^{31,64}, X. T. Huang⁵⁰, Y. P. Huang¹, Y. S. Huang⁵⁹, T. Hussain⁷⁴, F. Hölzken³, N. Hüsken³⁵, N. in der Wiesche⁶⁹, J. Jackson²⁷, S. Janchiv³², J. H. Jeong¹⁰, Q. Ji¹, Q. P. Ji¹⁹, W. Ji^{1,64}, X. B. Ji^{1,64}, X. L. Ji^{1,58}, Y. Y. Ji⁵⁰, X. Q. Jia⁵⁰, Z. K. Jia^{72,58}, D. Jiang^{1,64}, H. B. Jiang⁷⁷, P. C. Jiang^{46,h}, S. S. Jiang³⁹, T. J. Jiang¹⁶, X. S. Jiang^{1,58,64}, Y. Jiang⁶⁴, J. B. Jiao⁵⁰, J. K. Jiao³⁴, Z. Jiao²³, S. Jin⁴², Y. Jin⁶⁷, M. Q. Jing^{1,64}, X. M. Jing⁶⁴, T. Johansson⁷⁶, S. Kabana³³, N. Kalantar-Nayestanaki⁶⁵, X. L. Kang⁹, X. S. Kang⁴⁰, M. Kavatsyuk⁶⁵, B. C. Ke⁸¹, V. Khachatryan²⁷, A. Khoukaz⁶⁹, R. Kiuchi¹, O. B. Kolcu^{62A}, B. Kopf³, M. Kuessner³, X. Kui^{1,64}, N. Kumar²⁶, A. Kupsc^{44,76}, W. Kühn³⁷, J. J. Lane⁶⁸, L. Lavezzi^{75A,75C}, T. T. Lei^{72,58}, Z. H. Lei^{72,58}, M. Lellmann³⁵, T. Lenz³⁵, C. Li⁴⁷, C. Li⁴³, C. H. Li³⁹, Cheng Li^{72,58}, D. M. Li⁸¹, F. Li^{1,58}, G. Li¹, H. B. Li^{1,64}, H. J. Li¹⁹, H. N. Li^{56,j}, Hui Li⁴³, J. R. Li⁶¹, J. S. Li⁵⁹, K. Li¹, K. L. Li¹⁹, L. J. Li^{1,64}, L. K. Li¹, Lei Li⁴⁸, M. H. Li⁴³, P. R. Li^{38,k,l}, Q. M. Li^{1,64}, Q. X. Li⁵⁰, R. Li^{17,31}, S. X. Li¹², T. Li⁵⁰, W. D. Li^{1,64}, W. G. Li^{1,a}, X. Li^{1,64}, X. H. Li^{72,58}, X. L. Li⁵⁰, X. Y. Li^{1,64}, X. Z. Li⁵⁹, Y. G. Li^{46,h}, Z. J. Li⁵⁹, Z. Y. Li⁷⁹, C. Liang⁴², H. Liang^{1,64}, H. Liang^{72,58}, Y. F. Liang⁵⁴, Y. T. Liang^{31,64}, G. R. Liao¹⁴, Y. P. Liao^{1,64}, J. Libby²⁶, A. Limphirat⁶⁰, C. C. Lin⁵⁵, D. X. Lin^{31,64}, T. Lin¹, B. J. Liu¹, B. X. Liu⁷⁷, C. Liu³⁴, C. X. Liu¹, F. Liu¹, F. H. Liu⁵³, Feng Liu⁶, G. M. Liu^{56,j}, H. Liu^{38,k,l}, H. B. Liu¹⁵, H. H. Liu¹, H. M. Liu^{1,64},

Huihui Liu²¹, J. B. Liu^{72,58}, J. Y. Liu^{1,64}, K. Liu^{38,k,l}, K. Y. Liu⁴⁰, Ke Liu²², L. Liu^{72,58},
 L. C. Liu⁴³, Lu Liu⁴³, M. H. Liu^{12,g}, P. L. Liu¹, Q. Liu⁶⁴, S. B. Liu^{72,58}, T. Liu^{12,g},
 W. K. Liu⁴³, W. M. Liu^{72,58}, X. Liu^{38,k,l}, X. Liu³⁹, Y. Liu⁸¹, Y. Liu^{38,k,l}, Y. B. Liu⁴³,
 Z. A. Liu^{1,58,64}, Z. D. Liu⁹, Z. Q. Liu⁵⁰, X. C. Lou^{1,58,64}, F. X. Lu⁵⁹, H. J. Lu²³, J. G. Lu^{1,58},
 X. L. Lu¹, Y. Lu⁷, Y. P. Lu^{1,58}, Z. H. Lu^{1,64}, C. L. Luo⁴¹, J. R. Luo⁵⁹, M. X. Luo⁸⁰,
 T. Luo^{12,g}, X. L. Luo^{1,58}, X. R. Lyu⁶⁴, Y. F. Lyu⁴³, F. C. Ma⁴⁰, H. Ma⁷⁹, H. L. Ma¹,
 J. L. Ma^{1,64}, L. L. Ma⁵⁰, L. R. Ma⁶⁷, M. M. Ma^{1,64}, Q. M. Ma¹, R. Q. Ma^{1,64}, T. Ma^{72,58},
 X. T. Ma^{1,64}, X. Y. Ma^{1,58}, Y. M. Ma³¹, F. E. Maas¹⁸, I. MacKay⁷⁰, M. Maggiora^{75A,75C},
 S. Malde⁷⁰, Y. J. Mao^{46,h}, Z. P. Mao¹, S. Marcello^{75A,75C}, Z. X. Meng⁶⁷, J. G. Messchendorp^{13,65},
 G. Mezzadri^{29A}, H. Miao^{1,64}, T. J. Min⁴², R. E. Mitchell²⁷, X. H. Mo^{1,58,64}, B. Moses²⁷,
 N. Yu. Muchnoi^{4,c}, J. Muskalla³⁵, Y. Nefedov³⁶, F. Nerling^{18,e}, L. S. Nie²⁰, I. B. Nikolaev^{4,c},
 Z. Ning^{1,58}, S. Nisar^{11,m}, Q. L. Niu^{38,k,l}, W. D. Niu⁵⁵, Y. Niu⁵⁰, S. L. Olsen⁶⁴, S. L. Olsen^{10,64},
 Q. Ouyang^{1,58,64}, S. Pacetti^{28B,28C}, X. Pan⁵⁵, Y. Pan⁵⁷, A. Pathak³⁴, Y. P. Pei^{72,58},
 M. Pelizaeus³, H. P. Peng^{72,58}, Y. Y. Peng^{38,k,l}, K. Peters^{13,e}, J. L. Ping⁴¹, R. G. Ping^{1,64},
 S. Plura³⁵, V. Prasad³³, F. Z. Qi¹, H. Qi^{72,58}, H. R. Qi⁶¹, M. Qi⁴², T. Y. Qi^{12,g}, S. Qian^{1,58},
 W. B. Qian⁶⁴, C. F. Qiao⁶⁴, X. K. Qiao⁸¹, J. J. Qin⁷³, L. Q. Qin¹⁴, L. Y. Qin^{72,58},
 X. P. Qin^{12,g}, X. S. Qin⁵⁰, Z. H. Qin^{1,58}, J. F. Qiu¹, Z. H. Qu⁷³, C. F. Redmer³⁵, K. J. Ren³⁹,
 A. Rivetti^{75C}, M. Rolo^{75C}, G. Rong^{1,64}, Ch. Rosner¹⁸, S. N. Ruan⁴³, N. Salone⁴⁴, A. Sarantsev^{36,d},
 Y. Schelhaas³⁵, K. Schoenning⁷⁶, M. Scodreggio^{29A}, K. Y. Shan^{12,g}, W. Shan²⁴, X. Y. Shan^{72,58},
 Z. J. Shang^{38,k,l}, J. F. Shangguan¹⁶, L. G. Shao^{1,64}, M. Shao^{72,58}, C. P. Shen^{12,g}, H. F. Shen^{1,8},
 W. H. Shen⁶⁴, X. Y. Shen^{1,64}, B. A. Shi⁶⁴, H. Shi^{72,58}, H. C. Shi^{72,58}, J. L. Shi^{12,g}, J. Y. Shi¹,
 Q. Q. Shi⁵⁵, S. Y. Shi⁷³, X. Shi^{1,58}, J. J. Song¹⁹, T. Z. Song⁵⁹, W. M. Song^{34,1}, Y.
 J. Song^{12,g}, Y. X. Song^{46,h,n}, S. Sosio^{75A,75C}, S. Spataro^{75A,75C}, F. Stieler³⁵, S. S. Su⁴⁰,
 Y. J. Su⁶⁴, G. B. Sun⁷⁷, G. X. Sun¹, H. Sun⁶⁴, H. K. Sun¹, J. F. Sun¹⁹, K. Sun⁶¹, L. Sun⁷⁷,
 S. S. Sun^{1,64}, T. Sun^{51,f}, W. Y. Sun³⁴, Y. Sun⁹, Y. J. Sun^{72,58}, Y. Z. Sun¹, Z. Q. Sun^{1,64},
 Z. T. Sun⁵⁰, C. J. Tang⁵⁴, G. Y. Tang¹, J. Tang⁵⁹, M. Tang^{72,58}, Y. A. Tang⁷⁷, L. Y. Tao⁷³,
 Q. T. Tao^{25,i}, M. Tat⁷⁰, J. X. Teng^{72,58}, V. Thoren⁷⁶, W. H. Tian⁵⁹, Y. Tian^{31,64}, Z. F. Tian⁷⁷,
 I. Uman^{62B}, Y. Wan⁵⁵, S. J. Wang⁵⁰, B. Wang¹, B. L. Wang⁶⁴, Bo Wang^{72,58}, D. Y. Wang^{46,h},
 F. Wang⁷³, H. J. Wang^{38,k,l}, J. J. Wang⁷⁷, J. P. Wang⁵⁰, K. Wang^{1,58}, L. L. Wang¹,
 M. Wang⁵⁰, N. Y. Wang⁶⁴, S. Wang^{38,k,l}, S. Wang^{12,g}, T. Wang^{12,g}, T. J. Wang⁴³, W.
 Wang⁷³, W. Wang⁵⁹, W. P. Wang^{35,58,72,o}, X. Wang^{46,h}, X. F. Wang^{38,k,l}, X. J. Wang³⁹,
 X. L. Wang^{12,g}, X. N. Wang¹, Y. Wang⁶¹, Y. D. Wang⁴⁵, Y. F. Wang^{1,58,64}, Y. L. Wang¹⁹,
 Y. N. Wang⁴⁵, Y. Q. Wang¹, Yaqian Wang¹⁷, Yi Wang⁶¹, Z. Wang^{1,58}, Z. L. Wang⁷³,
 Z. Y. Wang^{1,64}, Ziyi Wang⁶⁴, D. H. Wei¹⁴, F. Weidner⁶⁹, S. P. Wen¹, Y. R. Wen³⁹,
 U. Wiedner³, G. Wilkinson⁷⁰, M. Wolke⁷⁶, L. Wollenberg³, C. Wu³⁹, J. F. Wu^{1,8}, L. H. Wu¹,
 L. J. Wu^{1,64}, X. Wu^{12,g}, X. H. Wu³⁴, Y. Wu^{72,58}, Y. H. Wu⁵⁵, Y. J. Wu³¹, Z. Wu^{1,58},
 L. Xia^{72,58}, X. M. Xian³⁹, B. H. Xiang^{1,64}, T. Xiang^{46,h}, D. Xiao^{38,k,l}, G. Y. Xiao⁴²,
 S. Y. Xiao¹, Y. L. Xiao^{12,g}, Z. J. Xiao⁴¹, C. Xie⁴², X. H. Xie^{46,h}, Y. Xie⁵⁰, Y. G. Xie^{1,58},
 Y. H. Xie⁶, Z. P. Xie^{72,58}, T. Y. Xing^{1,64}, C. F. Xu^{1,64}, C. J. Xu⁵⁹, G. F. Xu¹, H. Y. Xu^{67,2,p},
 M. Xu^{72,58}, Q. J. Xu¹⁶, Q. N. Xu³⁰, W. Xu¹, W. L. Xu⁶⁷, X. P. Xu⁵⁵, Y. Xu⁴⁰, Y. C. Xu⁷⁸,
 Z. S. Xu⁶⁴, F. Yan^{12,g}, L. Yan^{12,g}, W. B. Yan^{72,58}, W. C. Yan⁸¹, X. Q. Yan^{1,64}, H. J. Yang^{51,f},
 H. L. Yang³⁴, H. X. Yang¹, T. Yang¹, Y. Yang^{12,g}, Y. F. Yang⁴³, Y. F. Yang^{1,64}, Y. X. Yang^{1,64},
 Z. W. Yang^{38,k,l}, Z. P. Yao⁵⁰, M. Ye^{1,58}, M. H. Ye⁸, J. H. Yin¹, Junhao Yin⁴³, Z. Y. You⁵⁹,

B. X. Yu^{1,58,64}, C. X. Yu⁴³, G. Yu^{1,64}, J. S. Yu^{25,i}, M. C. Yu⁴⁰, T. Yu⁷³, X. D. Yu^{46,h},
Y. C. Yu⁸¹, C. Z. Yuan^{1,64}, J. Yuan³⁴, J. Yuan⁴⁵, L. Yuan², S. C. Yuan^{1,64}, Y. Yuan^{1,64},
Z. Y. Yuan⁵⁹, C. X. Yue³⁹, A. A. Zafar⁷⁴, F. R. Zeng⁵⁰, S. H. Zeng^{63A,63B,63C,63D}, X. Zeng^{12,g},
Y. Zeng^{25,i}, Y. J. Zeng^{1,64}, Y. J. Zeng⁵⁹, X. Y. Zhai³⁴, Y. C. Zhai⁵⁰, Y. H. Zhan⁵⁹,
A. Q. Zhang^{1,64}, B. L. Zhang^{1,64}, B. X. Zhang¹, D. H. Zhang⁴³, G. Y. Zhang¹⁹, H. Zhang⁸¹,
H. Zhang^{72,58}, H. C. Zhang^{1,58,64}, H. H. Zhang³⁴, H. H. Zhang⁵⁹, H. Q. Zhang^{1,58,64},
H. R. Zhang^{72,58}, H. Y. Zhang^{1,58}, J. Zhang⁸¹, J. Zhang⁵⁹, J. J. Zhang⁵², J. L. Zhang²⁰,
J. Q. Zhang⁴¹, J. S. Zhang^{12,g}, J. W. Zhang^{1,58,64}, J. X. Zhang^{38,k,l}, J. Y. Zhang¹, J. Z. Zhang^{1,64},
Jianyu Zhang⁶⁴, L. M. Zhang⁶¹, Lei Zhang⁴², P. Zhang^{1,64}, Q. Y. Zhang³⁴, R. Y. Zhang^{38,k,l},
S. H. Zhang^{1,64}, Shulei Zhang^{25,i}, X. M. Zhang¹, X. Y. Zhang⁴⁰, X. Y. Zhang⁵⁰, Y. Zhang⁷³,
Y. Zhang¹, Y. T. Zhang⁸¹, Y. H. Zhang^{1,58}, Y. M. Zhang³⁹, Yan Zhang^{72,58}, Z. D. Zhang¹,
Z. H. Zhang¹, Z. L. Zhang³⁴, Z. Y. Zhang⁴³, Z. Y. Zhang⁷⁷, Z. Z. Zhang⁴⁵, G. Zhao¹,
J. Y. Zhao^{1,64}, J. Z. Zhao^{1,58}, L. Zhao¹, Lei Zhao^{72,58}, M. G. Zhao⁴³, N. Zhao⁷⁹, R. P. Zhao⁶⁴,
S. J. Zhao⁸¹, Y. B. Zhao^{1,58}, Y. X. Zhao^{31,64}, Z. G. Zhao^{72,58}, A. Zhemchugov^{36,b}, B. Zheng⁷³,
B. M. Zheng³⁴, J. P. Zheng^{1,58}, W. J. Zheng^{1,64}, Y. H. Zheng⁶⁴, B. Zhong⁴¹, X. Zhong⁵⁹, H.
Zhou⁵⁰, J. Y. Zhou³⁴, L. P. Zhou^{1,64}, S. Zhou⁶, X. Zhou⁷⁷, X. K. Zhou⁶, X. R. Zhou^{72,58},
X. Y. Zhou³⁹, Y. Z. Zhou^{12,g}, Z. C. Zhou²⁰, A. N. Zhu⁶⁴, J. Zhu⁴³, K. Zhu¹, K. J. Zhu^{1,58,64},
K. S. Zhu^{12,g}, L. Zhu³⁴, L. X. Zhu⁶⁴, S. H. Zhu⁷¹, T. J. Zhu^{12,g}, W. D. Zhu⁴¹, Y. C. Zhu^{72,58},
Z. A. Zhu^{1,64}, J. H. Zou¹, J. Zu^{72,58}

¹ *Institute of High Energy Physics, Beijing 100049, People's Republic of China*

² *Beihang University, Beijing 100191, People's Republic of China*

³ *Bochum Ruhr-University, D-44780 Bochum, Germany*

⁴ *Budker Institute of Nuclear Physics SB RAS (BINP), Novosibirsk 630090, Russia*

⁵ *Carnegie Mellon University, Pittsburgh, Pennsylvania 15213, USA*

⁶ *Central China Normal University, Wuhan 430079, People's Republic of China*

⁷ *Central South University, Changsha 410083, People's Republic of China*

⁸ *China Center of Advanced Science and Technology, Beijing 100190, People's Republic of China*

⁹ *China University of Geosciences, Wuhan 430074, People's Republic of China*

¹⁰ *Chung-Ang University, Seoul, 06974, Republic of Korea*

¹¹ *COMSATS University Islamabad, Lahore Campus, Defence Road, Off Raiwind Road, 54000 Lahore, Pakistan*

¹² *Fudan University, Shanghai 200433, People's Republic of China*

¹³ *GSI Helmholtzcentre for Heavy Ion Research GmbH, D-64291 Darmstadt, Germany*

¹⁴ *Guangxi Normal University, Guilin 541004, People's Republic of China*

¹⁵ *Guangxi University, Nanning 530004, People's Republic of China*

¹⁶ *Hangzhou Normal University, Hangzhou 310036, People's Republic of China*

¹⁷ *Hebei University, Baoding 071002, People's Republic of China*

¹⁸ *Helmholtz Institute Mainz, Staudinger Weg 18, D-55099 Mainz, Germany*

¹⁹ *Henan Normal University, Xinxiang 453007, People's Republic of China*

²⁰ *Henan University, Kaifeng 475004, People's Republic of China*

²¹ *Henan University of Science and Technology, Luoyang 471003, People's Republic of China*

²² *Henan University of Technology, Zhengzhou 450001, People's Republic of China*

²³ *Huangshan College, Huangshan 245000, People's Republic of China*

²⁴ *Hunan Normal University, Changsha 410081, People's Republic of China*

²⁵ *Hunan University, Changsha 410082, People's Republic of China*

²⁶ *Indian Institute of Technology Madras, Chennai 600036, India*

²⁷ *Indiana University, Bloomington, Indiana 47405, USA*

- 28 *INFN Laboratori Nazionali di Frascati*, (A)*INFN Laboratori Nazionali di Frascati, I-00044, Frascati, Italy*; (B)*INFN Sezione di Perugia, I-06100, Perugia, Italy*; (C)*University of Perugia, I-06100, Perugia, Italy*
- 29 *INFN Sezione di Ferrara*, (A)*INFN Sezione di Ferrara, I-44122, Ferrara, Italy*; (B)*University of Ferrara, I-44122, Ferrara, Italy*
- 30 *Inner Mongolia University, Hohhot 010021, People's Republic of China*
- 31 *Institute of Modern Physics, Lanzhou 730000, People's Republic of China*
- 32 *Institute of Physics and Technology, Peace Avenue 54B, Ulaanbaatar 13330, Mongolia*
- 33 *Instituto de Alta Investigación, Universidad de Tarapacá, Casilla 7D, Arica 1000000, Chile*
- 34 *Jilin University, Changchun 130012, People's Republic of China*
- 35 *Johannes Gutenberg University of Mainz, Johann-Joachim-Becher-Weg 45, D-55099 Mainz, Germany*
- 36 *Joint Institute for Nuclear Research, 141980 Dubna, Moscow region, Russia*
- 37 *Justus-Liebig-Universität Giessen, II. Physikalisches Institut, Heinrich-Buff-Ring 16, D-35392 Giessen, Germany*
- 38 *Lanzhou University, Lanzhou 730000, People's Republic of China*
- 39 *Liaoning Normal University, Dalian 116029, People's Republic of China*
- 40 *Liaoning University, Shenyang 110036, People's Republic of China*
- 41 *Nanjing Normal University, Nanjing 210023, People's Republic of China*
- 42 *Nanjing University, Nanjing 210093, People's Republic of China*
- 43 *Nankai University, Tianjin 300071, People's Republic of China*
- 44 *National Centre for Nuclear Research, Warsaw 02-093, Poland*
- 45 *North China Electric Power University, Beijing 102206, People's Republic of China*
- 46 *Peking University, Beijing 100871, People's Republic of China*
- 47 *Qufu Normal University, Qufu 273165, People's Republic of China*
- 48 *Renmin University of China, Beijing 100872, People's Republic of China*
- 49 *Shandong Normal University, Jinan 250014, People's Republic of China*
- 50 *Shandong University, Jinan 250100, People's Republic of China*
- 51 *Shanghai Jiao Tong University, Shanghai 200240, People's Republic of China*
- 52 *Shanxi Normal University, Linfen 041004, People's Republic of China*
- 53 *Shanxi University, Taiyuan 030006, People's Republic of China*
- 54 *Sichuan University, Chengdu 610064, People's Republic of China*
- 55 *Soochow University, Suzhou 215006, People's Republic of China*
- 56 *South China Normal University, Guangzhou 510006, People's Republic of China*
- 57 *Southeast University, Nanjing 211100, People's Republic of China*
- 58 *State Key Laboratory of Particle Detection and Electronics, Beijing 100049, Hefei 230026, People's Republic of China*
- 59 *Sun Yat-Sen University, Guangzhou 510275, People's Republic of China*
- 60 *Suranaree University of Technology, University Avenue 111, Nakhon Ratchasima 30000, Thailand*
- 61 *Tsinghua University, Beijing 100084, People's Republic of China*
- 62 *Turkish Accelerator Center Particle Factory Group, (A)Istinye University, 34010, Istanbul, Turkey; (B)Near East University, Nicosia, North Cyprus, 99138, Mersin 10, Turkey*
- 63 *University of Bristol, (A)H H Wills Physics Laboratory; (B)Tyndall Avenue; (C)Bristol; (D)BS8 1TL*
- 64 *University of Chinese Academy of Sciences, Beijing 100049, People's Republic of China*
- 65 *University of Groningen, NL-9747 AA Groningen, The Netherlands*
- 66 *University of Hawaii, Honolulu, Hawaii 96822, USA*
- 67 *University of Jinan, Jinan 250022, People's Republic of China*
- 68 *University of Manchester, Oxford Road, Manchester, M13 9PL, United Kingdom*
- 69 *University of Muenster, Wilhelm-Klemm-Strasse 9, 48149 Muenster, Germany*
- 70 *University of Oxford, Keble Road, Oxford OX13RH, United Kingdom*
- 71 *University of Science and Technology Liaoning, Anshan 114051, People's Republic of China*
- 72 *University of Science and Technology of China, Hefei 230026, People's Republic of China*

- ⁷³ *University of South China, Hengyang 421001, People's Republic of China*
- ⁷⁴ *University of the Punjab, Lahore-54590, Pakistan*
- ⁷⁵ *University of Turin and INFN, (A)University of Turin, I-10125, Turin, Italy; (B)University of Eastern Piedmont, I-15121, Alessandria, Italy; (C)INFN, I-10125, Turin, Italy*
- ⁷⁶ *Uppsala University, Box 516, SE-75120 Uppsala, Sweden*
- ⁷⁷ *Wuhan University, Wuhan 430072, People's Republic of China*
- ⁷⁸ *Yantai University, Yantai 264005, People's Republic of China*
- ⁷⁹ *Yunnan University, Kunming 650500, People's Republic of China*
- ⁸⁰ *Zhejiang University, Hangzhou 310027, People's Republic of China*
- ⁸¹ *Zhengzhou University, Zhengzhou 450001, People's Republic of China*

^a *Deceased*

^b *Also at the Moscow Institute of Physics and Technology, Moscow 141700, Russia*

^c *Also at the Novosibirsk State University, Novosibirsk, 630090, Russia*

^d *Also at the NRC "Kurchatov Institute", PNPI, 188300, Gatchina, Russia*

^e *Also at Goethe University Frankfurt, 60323 Frankfurt am Main, Germany*

^f *Also at Key Laboratory for Particle Physics, Astrophysics and Cosmology, Ministry of Education; Shanghai Key Laboratory for Particle Physics and Cosmology; Institute of Nuclear and Particle Physics, Shanghai 200240, People's Republic of China*

^g *Also at Key Laboratory of Nuclear Physics and Ion-beam Application (MOE) and Institute of Modern Physics, Fudan University, Shanghai 200443, People's Republic of China*

^h *Also at State Key Laboratory of Nuclear Physics and Technology, Peking University, Beijing 100871, People's Republic of China*

ⁱ *Also at School of Physics and Electronics, Hunan University, Changsha 410082, China*

^j *Also at Guangdong Provincial Key Laboratory of Nuclear Science, Institute of Quantum Matter, South China Normal University, Guangzhou 510006, China*

^k *Also at MOE Frontiers Science Center for Rare Isotopes, Lanzhou University, Lanzhou 730000, People's Republic of China*

^l *Also at Lanzhou Center for Theoretical Physics, Key Laboratory of Theoretical Physics of Gansu Province, and Key Laboratory for Quantum Theory and Applications of MoE, Lanzhou University, Lanzhou 730000, People's Republic of China*

^m *Also at the Department of Mathematical Sciences, IBA, Karachi 75270, Pakistan*

ⁿ *Also at Ecole Polytechnique Federale de Lausanne (EPFL), CH-1015 Lausanne, Switzerland*

^o *Also at Helmholtz Institute Mainz, Staudinger Weg 18, D-55099 Mainz, Germany*

^p *Also at School of Physics, Beihang University, Beijing 100191, China*